AGU PUBLICATIONS

JGR

Journal of Geophysical Research: Atmospheres

RESEARCH ARTICLE
10.1002/2015JD023660

Key Points:
- New parameters for cloud conditions and boundary layer influence are applied
- The aerosol at 3580 m is strongly influenced by boundary layer injections
- Very little in situ production of cloud condensation nuclei is observed

Supporting Information:
- Figures S1–S4

Correspondence to:
E. Herrmann and M. Gysel,
erik.herrmann@iki.fi;
martin.gysel@psi.ch

Citation:
Herrmann, E., et al. (2015), Analysis of long-term aerosol size distribution data from Jungfraujoch with emphasis on free tropospheric conditions, cloud influence, and air mass transport, *J. Geophys. Res. Atmos.*, *120*, 9459–9480, doi:10.1002/2015JD023660.

Received 11 MAY 2015
Accepted 12 AUG 2015
Accepted article online 14 AUG 2015
Published online 17 SEP 2015

Analysis of long-term aerosol size distribution data from Jungfraujoch with emphasis on free tropospheric conditions, cloud influence, and air mass transport

Erik Herrmann[1], Ernest Weingartner[2], Stephan Henne[3], Laurent Vuilleumier[4], Nicolas Bukowiecki[1], Martin Steinbacher[3], Franz Conen[5], Martine Collaud Coen[4], Emanuel Hammer[1,6], Zsofia Jurányi[2], Urs Baltensperger[1], and Martin Gysel[1]

[1]Laboratory of Atmospheric Chemistry, Paul Scherrer Institute, Villigen, Switzerland, [2]Institute for Aerosol and Sensor Technology, University of Applied Sciences Northwestern Switzerland, Windisch, Switzerland, [3]Laboratory for Air Pollution/Environmental Technology, Swiss Federal Laboratories for Materials Science and Technology (Empa), Dübendorf, Switzerland, [4]Federal Office of Meteorology and Climatology (MeteoSwiss), Payerne, Switzerland, [5]Department of Environmental Sciences, University of Basel, Basel, Switzerland, [6]Now at Grolimund + Partner AG–environmental engineering, Bern, Switzerland

Abstract Six years of aerosol size distribution measurements between 20 and 600 nm diameters and total aerosol concentration above 10 nm from March 2008 to February 2014 at the high-alpine site Jungfraujoch are presented. The size distribution was found to be typically bimodal with mode diameters and widths relatively stable throughout the year and the observation period. New particle formation was observed on 14.5% of all days without a seasonal preference. Particles typically grew only into the Aitken mode and did not reach cloud condensation nucleus (CCN) sizes on the time scale of several days. Growth of preexisting particles in the Aitken mode, on average, contributed very few CCN. We concluded that the dominant fraction of CCN at Jungfraujoch originated in the boundary layer. A number of approaches were used to distinguish free tropospheric (FT) conditions and episodes with planetary boundary layer (PBL) influence. In the absence of PBL injections, the concentration of particles larger than 90 nm (N_{90}, roughly corresponding to the CCN concentration) reached a value ~40 cm^{-3} while PBL influence caused N_{90} concentrations of several hundred or even 1000 cm^{-3}. Comparing three criteria for free tropospheric conditions, we found FT prevalence for 39% of the time with over 60% during winter and below 20% during summer. It is noteworthy that a simple criterion based on standard trace gas measurements appeared to outperform alternative approaches.

1. Introduction

The high-alpine research station Jungfraujoch is located at 3580 m above sea level (asl) on the ridge between the peaks of Jungfrau and Mönch in the Bernese Alps in Switzerland. Aerosol measurements at Jungfraujoch first started in 1988 [*Baltensperger et al.*, 1997]. In the framework of the Global Aerosol Watch (GAW) program of the World Meteorological Organization, continuous measurements of aerosol optical properties have been performed since 1995 [*Collaud Coen et al.*, 2007].

Because it is frequently (~40%) inside clouds [*Baltensperger et al.*, 1998], Jungfraujoch has hosted numerous campaigns (e.g., Cloud and Aerosol Characterization Experiment, 2000–2014) to study cloud aerosol characteristics and cloud properties [e.g., *Henning et al.*, 2002; *Cozic et al.*, 2007; *Verheggen et al.*, 2007; *Sjogren et al.*, 2008; *Kamphus et al.*, 2010; *Ebert et al.*, 2011; *Hammer et al.*, 2014]. During such campaigns, there are typically measurements available to determine whether the site is inside the clouds, mostly through measurements of liquid water content. However, no such measurements are performed on a routine basis, i.e., in the context of the GAW monitoring observations. Mere observations of relative humidity (RH) do not suffice to establish cloud conditions as, especially in ice clouds, the RH (as referred to saturation water vapor pressure above liquid water) inside a cloud can be considerably below 100% [*Korolev and Isaac*, 2006]. To compensate for the lack of continuous cloud measurements, a parameter based on long-wave radiation was applied in this work.

Because of its altitude, Jungfraujoch is generally considered to be in the lower free troposphere for some or even —depending on season—much of the time [*Lugauer et al.*, 1998; *Henne et al.*, 2010; *Collaud Coen et al.*, 2011]. To

determine when background air masses are being sampled, various approaches have been applied over the years to estimate the influence of air masses from the planetary boundary layer (PBL). In a first approximation, the site was considered to be in the free troposphere (FT) during nighttime [e.g., *Nyeki et al*., 1998; *Weingartner et al*., 1999]. *Zellweger et al*. [2003] found the ratio of the sum of oxidized nitrogen species to carbon monoxide (NO_y/CO) to be a suitable approach to determine the age of an air mass, i.e., to identify fresh pollution transported to Jungfraujoch from the boundary layer. This method was subsequently used by several authors [e.g., *Zanis et al*., 2007; *Pandey Deolal et al*., 2013]. Also, radon-222 (^{222}Rn) with natural emissions from the land surface and a half-life of about 4 days has been used to assess PBL influence, most recently by *Griffiths et al*. [2014]. Finally, Lagrangian dispersion models (e.g., FLEXible PARTicle dispersion model (FLEXPART) [*Stohl et al*., 2005] and LAGRANTO [*Wernli and Davies*, 1997]) have been applied to determine air mass origins and boundary layer influence at Jungfraujoch [e.g., *Balzani Lööv et al*., 2008; *Tuzson et al*., 2011; *Uglietti et al*., 2011; *Sturm et al*., 2013; *Pandey Deolal et al*., 2014]. In this work, single tracers (^{222}Rn), tracer ratios (NO_y/CO), and dispersion modeling (FLEXPART) were compared to evaluate free troposphere conditions.

New particle formation (NPF) is a major source of climate-relevant cloud condensation nuclei [*Merikanto et al*., 2009]. At Jungfraujoch, the process has been studied with a neutral cluster and air ion spectrometer (NAIS) covering particles from 0.5 to 49 nm [*Boulon et al*., 2010]. While a detailed analysis of the first steps of nucleation and growth is beyond the scope of this work, the determination of the influence of NPF on CCN concentrations plays a significant role in our understanding of the Jungfraujoch aerosol.

Since 2008, particle number size distributions have been measured continuously at Jungfraujoch with a scanning mobility particle sizer (SMPS, diameter range 20–600 nm) system. While some long time series of aerosol size distribution measurements are available today (e.g., at SMEAR II [*Nieminen et al*., 2014], at Puy de Dôme [*Venzac et al*., 2009], on Tenerife [*García et al*., 2014], on Antarctica [*Fiebig et al*., 2014], and on Finokalia [*Kalivitis et al*., 2015]), our data represent a unique set of high-alpine observations.

In this paper, we present 6 years of particle size distribution observations to complement previous long-term studies at Jungfraujoch concerning aerosol optical properties [*Collaud Coen et al*., 2007, 2011], cloud condensation nuclei [*Jurányi et al*., 2011], and Saharan dust events [*Collaud Coen et al*., 2004]. Furthermore, we aim to update and extend on the only dedicated SMPS publication about Jungfraujoch aerosol by *Weingartner et al*. [1999]. As laid out above, this data set was studied in regard to FT/PBL distinction, cloud influence, and the influence of particle formation on CCN-sized particle concentrations. The synthesis of these methods made a reliable description of the aerosol at Jungfraujoch possible.

2. Methods

2.1. Site and Aerosol Measurements

At 3580 m asl (46°33′N, 7°59′E) on a ridge between two mountains higher than 4000 m, Jungfraujoch is well away from major anthropogenic pollution sources and thus nominally considered a background site. However, local pollution from construction activities is sporadically possible, and tourism-related emissions occur especially during periods of favorable weather conditions and during the months of June to September. As the focus of this work is not on local pollution, data potentially influenced by local activities were removed from further analysis by visual inspection of the single size distribution spectra. This is based on the assumption that drastic, short-lived fluctuations in aerosol properties at a remote site such as Jungfraujoch are most likely caused by local pollution. This contamination is driven by tourism, which means that incident frequency depends on weather conditions and thus season. During the most polluted days of summer, up to 10% of data needed to be discarded.

The aerosol inlet of the Sphinx laboratory at Jungfraujoch was described in detail by *Weingartner et al*. [1999]. In short, the heated (~20°C) inlet is designed to collect all aerosol particles and cloud droplets up to 40 μm at wind speeds up to 20 m s^{-1}. It evaporates all condensed water to measure interstitial as well as activated aerosol particles. Losses for the whole inlet system are below 5% for particles between 10 and 750 nm diameters. Inside the laboratory, the dried aerosol stream is distributed to a series of instruments (currently 10) which are monitoring aerosol properties as part of the GAW network. These are complemented by a number of additional instruments when intensive field campaigns are performed at the Sphinx.

Relevant for this work are a scanning mobility particle sizer (SMPS) and a condensation particle counter (CPC). The custom-built SMPS consists of a differential mobility analyzer (DMA, TSI 3071) and a CPC (TSI 3775) and measures aerosol size distributions between 20 and 600 nm in diameter with a time resolution of 6 min (up scan time 300 s). The sample flow is 0.3 L min^{-1} as determined by the CPC's sample flow. The sheath flow is 3 L min^{-1}, arranged in a closed-loop setup and controlled by a mass flow controller coupled with pressure and temperature sensors. SMPS data treatment was described extensively by *Jurányi et al*. [2011]. The instrument and data inversion routines were tested in an intercomparison exercise [*Wiedensohler et al*., 2012]. Over the whole measurement period, the integral SMPS count and the CPC count typically agreed within 15%. Periods with over 20% discrepancy have been removed from further data analysis.

The present work analyzes data from March 2008 to February 2014, i.e., a period of 6 years. Data gaps due to instrument failure, poor data quality, or scheduled maintenance amount to roughly 10% (detailed data coverage can be inferred from Figure 3). All SMPS data used in this work are or will be available in the EBAS database of the European Monitoring and Evaluation Programme at http://ebas.nilu.no/.

In addition to the size distribution measurements, a CPC (TSI 3772, cutoff diameter of 10 nm) monitors the total aerosol number concentration above 10 nm with a time resolution of 1 min at a sample flow rate of 1 L min^{-1}. As there are typically very few particles larger than 600 nm (see Figure S1 in the supporting information), these data can be used together with the SMPS data to estimate the number of particles between 10 and 20 nm (N_{10-20}). Due to somewhat higher diffusion losses for small particles [*Weingartner et al*., 1999] and the nonideal cutoff curve of any CPC, this N_{10} will underestimate the true concentration of particles between 10 and 20 nm but, nevertheless, provide useful information on the concentration of small particles especially during new particle formation events.

2.2. Meteorological Data and Cloud Criteria

All meteorological instruments are part of the SwissMetNet network of MeteoSwiss. The temperature and humidity are measured by a Thygan (Meteolabor). The latter is also measured by a high-precision dew point mirror. The wind components are measured by a Rosemount pitot tube (Raytheon) on a 10 m mast. Sunshine duration measurements are performed with an electronic Haenni Solar 111B (S-111B) [*Philipona et al*., 1993].

Monitoring of long-wave downward irradiance flux (LWD) has been performed with thermopile-based pyrgeometers. Operational procedures similar to those mandated by the Baseline Surface Radiation Network (BSRN) [*McArthur*, 2005] have been used, except for daily maintenance requirements, due to the remote nature of the site. Since 2008, the measurements have been performed with one Kipp and Zonen CG4 pyrgeometer [*Kipp and Zonen*, 2014] and one Eppley PIR pyrgeometer with a three-thermistor dome temperature measurement modification [*Philipona et al*., 2001]. The redundant measurements are sampled at 1 Hz frequency, and the corresponding 1 min statistics (average, standard deviation, minimum, and maximum) are recorded. All data loggers are synchronized several times per hour to the same time server. Absolute standards have been developed for LW radiation [*Philipona et al*., 2001; *Gröbner et al*., 2014]. As a consequence, BSRN absolute accuracy targets of 2% or 3 W m^{-2} (greatest of the two limits) have been shown to be reachable for calibration precision. Such uncertainty is representative of the calibration uncertainty and not of the actual operational observation uncertainty, which includes additional sources. In particular, at high-altitude stations, especially those that are frequently within clouds, a particular challenge is keeping the instrument domes free of water (liquid or solid), because of the high LW emissivity of water. The uncertainty of LWD irradiance at Jungfraujoch should be considered at least twice the BSRN accuracy targets.

From long-wave radiation (LW) measurements it is possible to determine the corresponding effective sky temperature using the relation

$$\mathrm{LW} = \sigma_{\mathrm{LW}} \cdot T^4 \tag{1}$$

where $\sigma_{\mathrm{LW}} = 5.67 \cdot 10^{-8}\,\mathrm{W\,m^{-2}\,K^{-4}}$. Comparing this "sky temperature" to ambient temperature provides the means to determine whether the measurement site is inside clouds: for clouds, one expects to find that $T_{\mathrm{sky}} \approx T_{\mathrm{ambient}}$; outside of clouds, one expects T_{sky} to be considerably lower. Figure 1 shows a comparison of ambient and sky temperatures for the whole measuring period with a time resolution of 6 min and split into seasons. One can clearly see how the data points form two distinct clusters. The one along and slightly below the 1:1 line is interpreted as in-cloud conditions. On the black dotted line, the difference

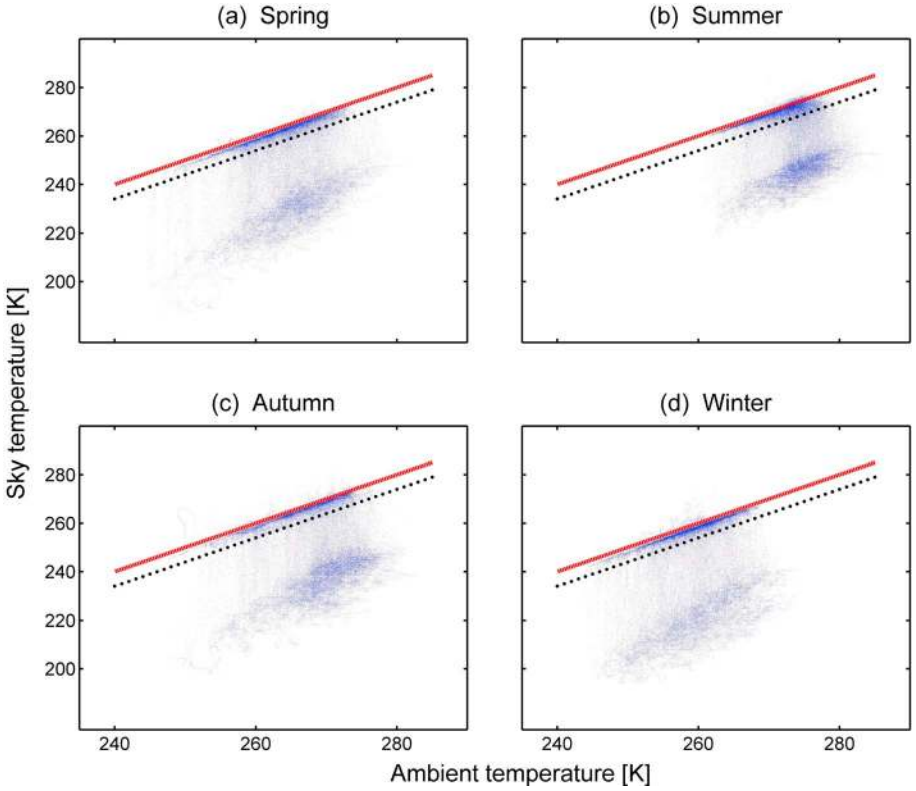

Figure 1. Comparison of sky temperature and ambient temperature for the 6 years of data analyzed in this work (March 2008 to February 2014), split into seasons. The data points form two clusters signifying in-cloud (upper cluster on the red 1:1 line) and cloud-free (lower cluster) conditions. The remaining points can be interpreted as clouds above the site or patchy clouds. All data points below the black dotted line ($T_{sky} - T_{ambient} = 6$ K) have been considered to be out of cloud.

between sky and ambient temperature is 6 K. In this work, everything above this line is considered in-cloud, and everything below it out-of-cloud. Out-of-cloud conditions include clouds above the site at different heights, patchy clouds, and clear-sky situations. The latter is represented by the second cluster of data points well below the 1:1 line. The value of 6 K was chosen to capture the complete in-cloud cluster while at the same time including as little out-of-cloud data points as possible. Of course, some degree of ambiguity cannot be avoided when determining this limit. Nevertheless, the sky temperature approach offers a fairly clear distinction between in-cloud and out-of-cloud situations in the absence of actual cloud measurements. The alternative approach to use RH as a cloud parameter does not provide such a good quality distinction as it is unreliable for fully glaciated clouds whose RH can vary significantly and can be well below 100% [*Korolev and Isaac*, 2006]. For the comparison, clouds were assumed to be present when RH > 97%. For RH values below 95%, we assumed the station to be outside of clouds. Naturally, the exact choice of these limits can be discussed but tests have shown that shifts of 1 K or 1% do not significantly alter the results.

Since 2011, a public high-resolution panorama webcam has been operational at the Sphinx laboratory (www.switch.ch), overlooking the entire surroundings from S to W to N. The panorama is automatically updated every full hour. In the present study these pictures were used to estimate the presence of a cloud at the Sphinx laboratory. To produce a continuous time series we assumed that each panorama represents one full hour. For this purpose the panorama picture was divided in three subpictures that show a high color contrast (dark rock formations surrounded by white snow and blue sky) during daytime clear weather conditions. During the presence of clouds these picture subsets show a uniform white color. The difference between the two conditions was mathematically captured by calculating the standard deviation of the RGB (red, green, and blue) color pixels (1 standard deviation per color). Standard deviation threshold criteria for the presence of clouds were set by visual inspection and confirmation of a sufficient number (>500) of panorama

pictures. The results of this analysis were used in comparison to the cloud criteria derived from sky temperature and relative humidity. One has to point out that various cameras are available at Jungfraujoch [e.g., *Wacker et al*., 2015]. For this work, we used the SWITCH webcam as it offers the best currently available compromise between data coverage, time resolution, and accuracy of the cloud determination algorithm.

2.3. Gas Phase Measurements

A large suite of continuous trace gas observations at Jungfraujoch is run by the Swiss Federal Laboratories for Materials Science and Technology (Empa) as part of the operation of the Swiss National Air Pollution Monitoring Network. The species used in the present study are carbon monoxide (CO) and the sum of oxidized nitrogen species (NO_y). From 1996 until spring 2014, CO has been measured at Jungfraujoch with commercially available instruments (Horiba APMA-360 and APMA-370, Kyoto, Japan) using the cross flow modulated non-dispersive infrared absorption technology (NDIR) [*Zellweger et al*., 2009]. In September 2011, a cavity ringdown spectrometer (Picarro Inc., G2401) was deployed at Jungfraujoch next to the NDIR analyzer, which became the master instrument in January 2012 due to its superior performance [*Zellweger et al*., 1997]. For both types of CO analyzers, the sample air was dried prior to analysis to reduce potential water vapor interferences. NO_y was measured with a highly sensitive nitrogen monoxide (NO) analyzer with chemiluminescence detector (Eco Physics CLD89p) after conversion of NO_y to NO on a heated gold catalyst (300°C) in the presence of 2% CO as a reducing agent [*Pandey Deolal et al*., 2012].

Radon-222 was measured with a two-filter dual flow loop instrument based on the design by *Whittlestone and Zahorowski* [1998]. It has a delay chamber of 400 L to remove thoron and a radon detection chamber of 750 L. Radon measurements at Jungfraujoch are discussed in *Griffiths et al*. [2014].

2.4. Lagrangian Backward Simulations

We used backward Lagrangian particle dispersion simulations to characterize the history of sampled air masses and to obtain a transport categorization. The Lagrangian particle dispersion model FLEXPART (version 9.01) [*Stohl et al*., 2005] was used to calculate source receptor relationships (SRRs) of a passive air tracer for the full SMPS observation period covered in this work. For each 3-hourly interval within this period 50,000 particles were released at the receptor site Jungfraujoch and traced back in time for 10 days considering transport by the mean flow, turbulence, and deep convection. The model was driven by European Centre for Medium-Range Weather Forecast operational analyses (00:00, 06:00, 12:00, 18:00 UTC) and forecasts (03:00, 09:00, 15:00, 21:00 UTC) with 91 vertical levels and a horizontal resolution of $1° \times 1°$ for the global domain and $0.2° \times 0.2°$ for a nested domain covering the Alpine area (4°W–16°E, 39°–51°N). After 25 June 2013, 137 vertical model levels were available. A release height of 3000 m was chosen for Jungfraujoch, which is significantly lower than the true altitude of the observatory. The limited horizontal resolution of the model requires a smoothed model topography that does not represent the Alpine topography very well and gives a model ground at approximately 2500 m asl at the location of Jungfraujoch. A release height somewhere between the station's real altitude and the model ground needs to be selected and for Jungfraujoch the choice of 3000 m asl proved to provide best model performance [*Brunner et al*., 2012; *Keller et al*., 2012].

The simulated SRRs allow directly linking a mass release at a source location with a mass mixing ratio at the receptor [*Seibert and Frank*, 2004]. SRRs are given in units of $s\,m^3\,kg^{-1}$ and are also referred to as footprints and emission sensitivities. SRRs were generated on a regular grid with $0.1° \times 0.1°$ horizontal resolution covering western Europe. By multiplication of the SRRs with emission inventories and summation over the entire output grid, time series of mixing ratios of CO, CH_4, and anthropogenic CO_2 were derived for Jungfraujoch. Emissions were taken from the Emission Database for Global Atmospheric Research (EDGAR) inventory (EC-JRC/PBL.EDGAR version 4.2; http://edgar.jrc.ec.europa.eu/) [*Olivier and Berdowski*, 2001] for the reference year 2008. The simulated mixing ratios give the enhancement of the respective trace gas during the period of transport but do not include a baseline mixing ratio.

Based on nighttime CO footprints, we derived a threshold to describe what level of enhancement can be considered a significant PBL influence. The basic assumption is that Jungfraujoch is mostly free from PBL influence during the night. Allowing for a few instances of extreme meteorological conditions, we chose the threshold in such a way that Jungfraujoch during the night is in the free troposphere for 99% of the cases. This threshold was then used to determine for each 3 h period when the last PBL contact has occurred

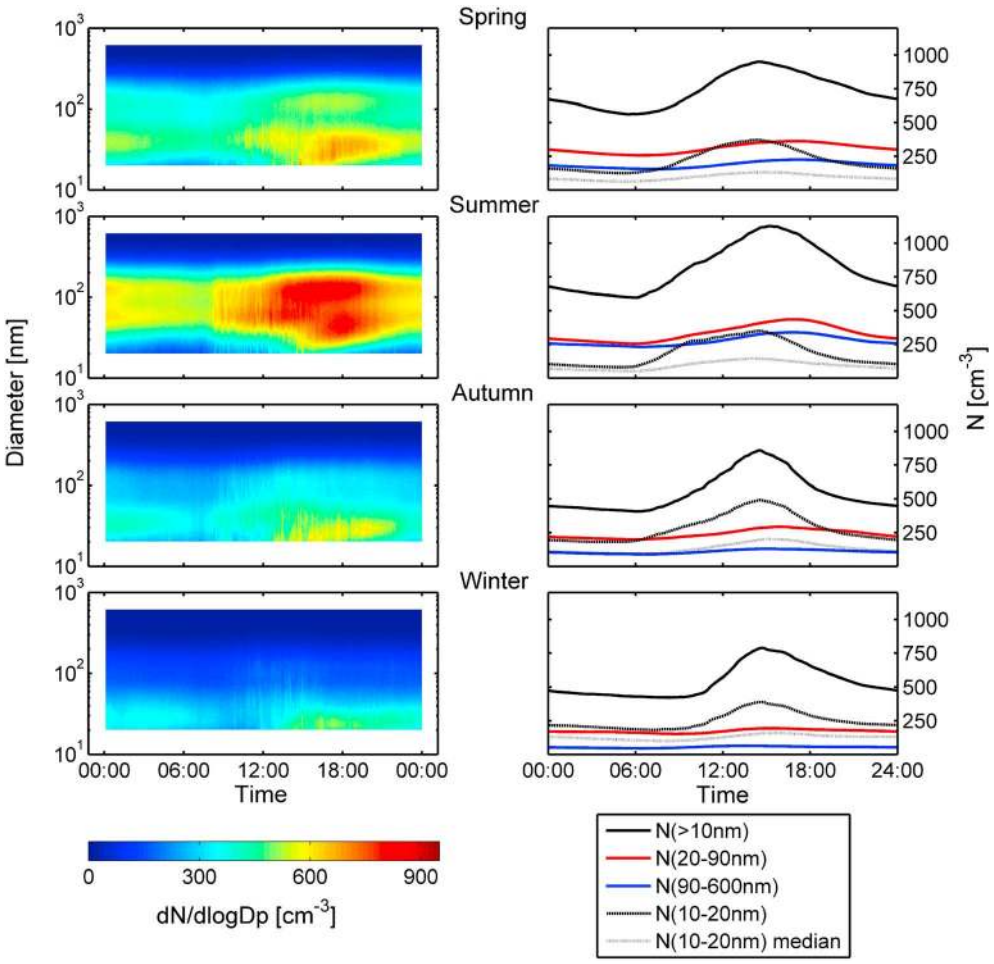

Figure 2. Mean diurnal size distribution for the different seasons (left column) and diurnal cycles for $N(>10$ nm), $N(20–90$ nm), $N(90–600$ nm), and $N(10–20$ nm), approximately representing total N, Aitken mode, accumulation mode, and part of the nucleation mode, respectively. The difference between the mean and median of $N_{10–20}$ illustrates the influence of nucleation events that occur on average every 6th or 7th day and cause a strong increase of $N_{10–20}$.

(time since PBL). Using CO instead of pure SRRs focuses this analysis on contacts with the PBL that was polluted by combustion processes. Influences from natural precursor emissions from areas with low CO emissions might be missed by the present analysis.

3. Results

3.1. Size Distribution Characteristics

Figure 2 shows the mean diurnal cycle of number size distributions for the different seasons in the left column and cycles of integrated number concentration in different size fractions on the right. To complement these data, Figure S2 shows average size distributions for the seasons, offering an additional viewpoint. In these figures, and in the context of this work, in general, spring includes the months March, April, and May; summer is June, July, and August; autumn covers September, October, and November; and, finally, December, January, and February make up winter. While the median would possibly be a better choice to minimize the effect of outliers and thus show a typical day, we have chosen means to also include the effect of new particle formation in this figure. Such events are observed on only a small fraction of days (see section 3.5) and would thus be suppressed by the median approach. In the right column, we show partial sums of the size distribution and additional information provided from the total aerosol count above 10 nm. We have split the size distribution at 90 nm diameter with the sum from 20 to 90 nm approximating the Aitken mode and the sum from 90 to 600 nm roughly representing the accumulation mode. While the

lower limit of the accumulation mode is not entirely well defined in the literature (e.g., 80 nm in *Baron and Willeke* [2005] and 100 nm in *Seinfeld and Pandis* [2006]), we chose a threshold of 90 nm as this corresponds to the average threshold diameter that determines whether particles act as CCN in liquid clouds at Jungfraujoch [*Hammer et al*., 2014]. This means that $N(>90\,\text{nm}) = N_{90}$ is not only a possible approximation of the accumulation mode concentration but indeed a significant variable in terms of the aerosol particles' climate relevance (aerosol-cloud interaction, previously termed indirect aerosol effect).

In both columns of Figure 2, we clearly see that summer ($N_{10} = 1120\,\text{cm}^{-3}$; $N_{90} = 290\,\text{cm}^{-3}$) has the highest particle concentrations and winter ($N_{10} = 790\,\text{cm}^{-3}$; $N_{90} = 70\,\text{cm}^{-3}$) the lowest, with spring ($N_{10} = 950\,\text{cm}^{-3}$; $N_{90} = 220\,\text{cm}^{-3}$) and autumn ($N_{10} = 860\,\text{cm}^{-3}$; $N_{90} = 130\,\text{cm}^{-3}$) in between. Spring characteristics appear to be closer to summer and autumn closer to winter. The bimodality of the average size distributions is most prominent in summer and spring while winter shows very low concentrations in the accumulation mode. The parameters on the right underline certain features also visible on the left. For example, we see a slight decrease in the total particle concentration during the early hours of the day before sunrise which is likely related to descending airflow induced by diabatic surface cooling and resulting downslope flow, leading to low particle loads characteristic of free tropospheric conditions. As hardly any accumulation mode particles are formed at Jungfraujoch (see section 3.5 for details), the diurnal cycles of N_{90} give a first estimate of boundary layer influence. In winter, N_{90} is almost completely flat, indicating that there is only very little PBL influence as already shown in previous studies [e.g., *Zellweger et al*., 2003]. Naturally, summer shows the most significant influence of injections from the boundary layer.

The diurnal cycle of the total aerosol concentration above 10 nm is strongly driven by the cycle of the small particles between 10 and 20 nm. This is most obvious for the winter months when the accumulation mode and the Aitken mode show only little variation during the day. Small particles, however, have a very distinct cycle in winter as well as in all other seasons, indicating that new particle formation at or near Jungfraujoch plays a significant role for the number concentration of small particles ($D_p < 20$ nm) all around the year. The peak in the small particle cycle is widest in summer and spring and comparatively narrow in winter. This reflects the central role of radiation to drive the chemistry that produces the condensable matter from the volatile precursor vapors that are necessary for particles to form: during winter, the necessary vapors can be produced only during a few hours each day while sunlight is available for much longer during summer and spring. Radiation also causes longer boundary layer influence during summer days; i.e., condensable vapors or their precursors that originate in the PBL and are necessary for new particle formation are available for a longer time. To better illustrate the influence of nucleation events we have included both the mean and median number concentration of particles between 10 and 20 nm (N_{10-20}) in the panels on the right. The effect of new particle formation, which causes a strong increase of N_{10-20} around every 5th to 10th day, is essentially suppressed in the median, resulting in a much flatter diurnal cycle when compared to the mean. The panels on the right show the diurnal variability of small particles below 20 nm from a mean and from a median point of view. The median indicates the contribution of (nonnucleation) transport from the PBL to the diurnal cycle, while the mean shows the dominant influence of new particle formation.

To further characterize the evolution of the size distribution during the observation period and identify annual cycles we fitted a multimodal lognormal size distribution to hourly SMPS data following the algorithm described by *Hussein et al*. [2005]. As the fitting of a nucleation mode was not always possible and even successful fits cannot be considered very trustworthy due to size range limitations, we present only Aitken and accumulation mode fit parameters in Figure 3. For this figure, we have chosen a moving 30 day median. In addition to the parameters of the fitted modes (geometric mean diameter, total number concentration, and geometric standard deviation), these statistical parameters are shown for the whole measured size distribution from 20 to 600 nm. Figure 3a shows Aitken and accumulation mode diameters and, oscillating between these two, the geometric mean diameter. During the winter season, this geometric mean diameter is very close to the Aitken mode diameter, reflecting the fact that accumulation mode concentrations are very low during those periods (see Figures 2 and 3b). Aitken and accumulation mode diameters show no distinctive seasonal pattern and appear to be relatively stable throughout the observations. For the 6 year measurement period, we found a mean Aitken mode diameter of 45 nm (median 46 nm) with a standard deviation of 11 nm based on 1 h distributions. For the accumulation mode, these values are 135 nm, 131 nm, and 26 nm, respectively. The values are very similar to those observed by *Weingartner et al*. [1999] who obtained values of 43 ± 3 nm and 140 ± 6 nm for Aitken and accumulation modes, respectively, for 1 year of SMPS observations at Jungfraujoch in 1997/1998.

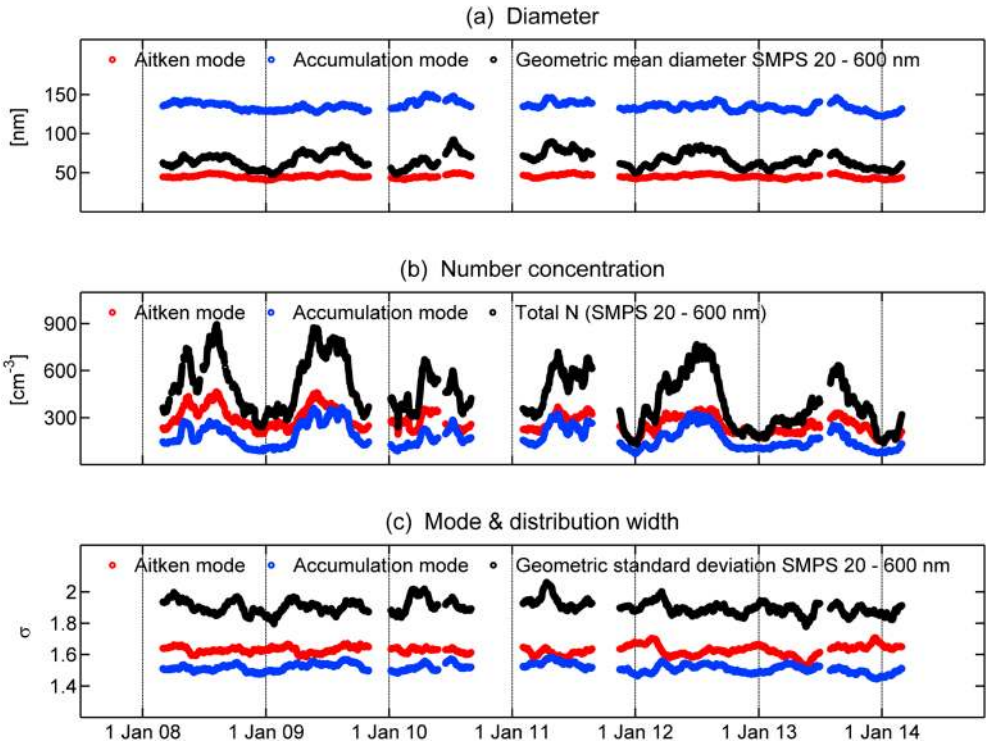

Figure 3. Mode parameters from multimodal lognormal fits for Aitken and accumulation modes and respective values for the whole size distribution between 20 and 600 nm diameters. Running 30 day medians over 1 h data are shown.

The number concentrations indicate a clear annual pattern with maxima during the summer and minima in the winter. This applies to the Aitken and accumulation modes as well as to the total number concentration. The annual cycle is most distinct for the accumulation mode, which shows very low concentrations during winter (below 50 cm^{-3}) and comes close to Aitken mode concentrations (300 cm^{-3}) during some summers (also compare to Figure 2). It is noteworthy that particle concentrations vary considerably from year to year, with total N reaching 900 cm^{-3} during some summers while hardly exceeding 600 cm^{-3} during others. Similar observations can be made for concentrations in both modes. This is most likely caused by meteorological variability which influences the frequency and intensity of the transport of boundary layer air to Jungfraujoch as *Collaud Coen et al.* [2011] have shown. Only the winter low of the accumulation mode appears rather consistent throughout the 6 years, as vertical transport has generally a low impact in winter.

Finally, no pattern can be discerned for the mode width (geometric standard deviation). We find $\sigma_{Aitken} = 1.63 \pm 0.15$ for the Aitken mode and $\sigma_{Accu} = 1.52 \pm 0.14$ for the accumulation mode. These are somewhat smaller than the values reported by *Weingartner et al.* [1999], which were 2.13 ± 0.11 and 1.61 ± 0.03 for the Aitken and accumulation modes, respectively. For σ_{Aitken}, the difference is statistically significant. As the figure illustrates, even the geometric standard deviation of the whole size distribution from 20 to 600 nm stays below the reported value for σ_{Aitken} and amounts to only 1.90 ± 0.17. Different fitting strategies may be responsible for this difference as our fits are based on hourly values, whereas *Weingartner et al.* [1999] performed multimodal fits for average distributions based on much larger data sets. The larger standard deviations for the mode diameters found here support this view: averaging over a large set of size distributions with small σ and varying diameters will result in a size distribution with a larger σ. However, with over 10 years between these observations, one cannot exclude actual changes in the aerosol characteristics, and all possible explanations thus have to remain speculation.

3.2. Influence of Clouds

To assess the properties of the particle size distribution inside and outside of clouds, three different cloud criteria were compared (see section 2.2 for details on the cloud criteria). The fraction of in-cloud conditions obtained from the webcam, sky temperature, and ambient RH-based criteria are listed in Table 1. As the table

Table 1. Prevalence of In-Cloud Conditions During the Different Seasons for Various Cloud Parameters[a]

		In Cloud (%)
Spring	Webcam	50
	Sky temperature	47
	Relative humidity	12
Summer	Webcam	30
	Sky temperature	38
	Relative humidity	20
Autumn	Webcam	28
	Sky temperature	33
	Relative humidity	15
Winter	Webcam	38
	Sky temperature	38
	Relative humidity	5
Total	Webcam	37
	Sky temperature	40
	Relative humidity	14

[a]As for Figure 4, only daytime data starting from 2011 were used.

shows, sky temperature and webcam criteria provide very similar results for all seasons. For the overall cloud percentage they yield 40% and 37%, respectively, which agree well with the previously reported cloud fraction of 40% based on in situ cloud observations [*Baltensperger et al.*, 1998]. The RH criterion, however, fails to identify cloud conditions during all seasons as Table 1 shows. This is likely caused by the fact that temperatures at the site are mostly below 0°C. Accordingly, the RH method works best during summer when the retrieved cloud percentage is closest to the other methods. However, also during summer, the RH criterion differs very significantly from the other approaches. Overall, the use of this approach retrieves in-cloud conditions for only 14% of the time, which is in contrast to the other criteria and earlier findings. As argued in section 2.2, this criterion is expected to be least reliable, particularly for fully glaciated clouds.

Figure 4 shows the cloud effect on the median size distributions with respect to the different cloud criteria based on webcam pictures, sky temperature, and relative humidity (see section 2.2). The webcam-based cloud criterion is only available from October 2011 onward, and it is less reliable for nighttime. To ensure comparability, we have limited the analysis of all-cloud criteria in Figure 4 to this period. Thus, Figure 4 shows only daytime data from autumn 2011 onward. However, tests have shown very similar results for the omitted periods; i.e., the cloud effects shown in the figure can be considered to apply in general. The distinction between in-cloud and out-of-cloud situations produces generally very similar results when using webcam and sky temperature criteria. Using the RH criterion provides qualitatively similar results for the cloud effect on size distribution, while some quantitative differences appear for example in spring (Figure 4a). This assessment is consistent with the above conclusion that sky temperature and webcam pictures are more reliable criteria to determine in-cloud conditions than ambient RH.

A notable difference between webcam and sky temperature approaches is evident in autumn (Figure 4c), when the webcam criterion suggests a nucleation mode (roughly until 25…30 nm diameter) for in-cloud conditions, while the sky temperature parameter sees this nucleation mode outside of clouds. Of course, we would not expect a nucleation mode for in-cloud conditions, as the large condensation sink offered by the cloud droplets absorbs the condensable vapors. This finding illustrates the limitations of the webcam parameter which extrapolates one snapshot to cover a full hour. In conditions of patchy clouds and at cloud edges, i.e., locally quickly changing conditions, this approach is likely to produce false positives. This observation also hints at the possibility of new particle formation events related to cloud evaporation at Jungfraujoch. Such events have been observed with airplanes at the top of clouds [*Clarke et al.*, 1998]. Some disagreement between webcam and sky temperature criteria can also be seen for the inside cloud size distributions in summer (Figure 4b). Comparing Figure 4 and the relevant numbers in Table 1, it appears that the sky temperature parameter classifies a certain amount of out-of-cloud size distribution spectra as in-cloud. As Figure 1b illustrates, the comparison of sky and ambient temperature in summer produces a somewhat less well defined in-cloud cluster of data points. In summer, the cloud base is frequently above Jungfraujoch. When the distance to the cloud is small, the difference between sky temperature and ambient temperature at Jungfraujoch will also be small. For these cases, the sky temperature parameter cannot distinguish between in-cloud and out-of-cloud conditions. Nevertheless, the data presented in Table 1 and Figure 4 show that the sky temperature is a good parameter to determine cloud conditions at Jungfraujoch in the majority of cases.

As we have found the relative humidity to be an unreliable parameter, we will discuss the features of the size distributions and their differences with respect to cloud conditions only for sky temperature and webcam

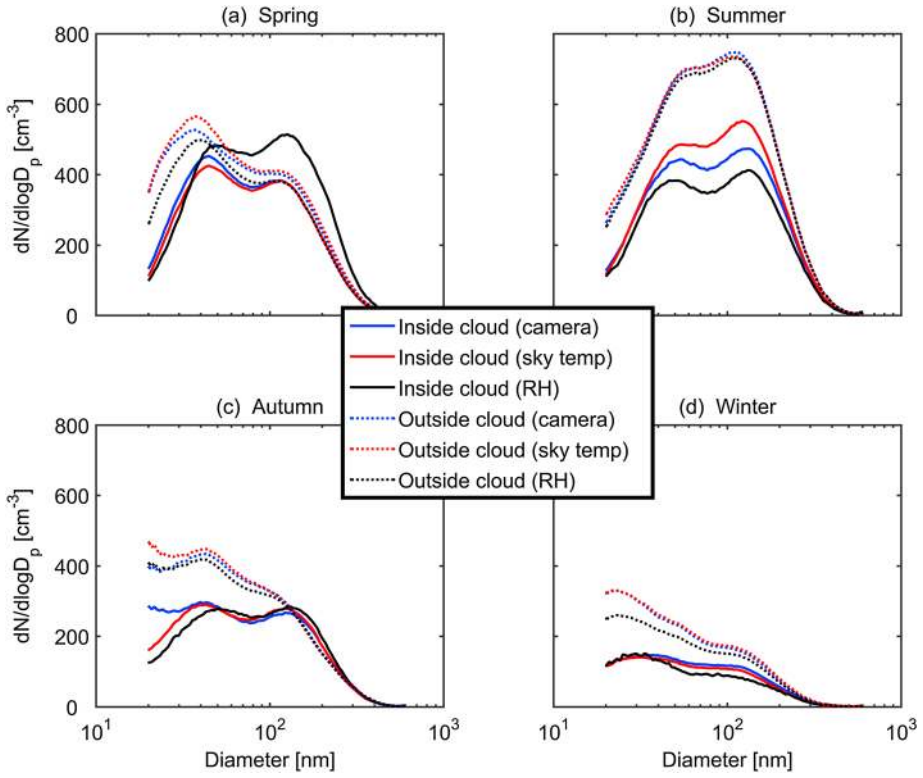

Figure 4. Seasonal median aerosol size distributions for in-cloud and out-of-cloud conditions, as derived by different classification tools. Only daytime data starting from 2011 were used (see section 3.2), but the full data set yield similar results. The vertical line at 90 nm (mean cloud droplet activation limit) was included for orientation.

parameters. Generally, the aerosol number concentrations are higher for out-of-cloud conditions compared to in-cloud conditions. This contradicts earlier results by *Weingartner et al*. [1999], but since their data cover only a few months, weather conditions can have a very pronounced effect on the findings. The difference we found between in-cloud and out-of-cloud situations is larger for the Aitken mode compared to the accumulation mode, and it also depends on season. In spring, the main difference between in-cloud and out-of-cloud conditions is seen in the Aitken mode. It has higher particle concentrations and is shifted to smaller particles when the site is out of clouds. This is likely caused by new particle formation which is suppressed inside clouds. Inside clouds, scavenging of Aitken mode particles can diminish their concentration. For the accumulation mode, the median spring size distributions show no significant differences between in-cloud and out-of-cloud conditions. Of course, some of the sampled spring clouds have most likely been affected by cloud processing. However, transport to Jungfraujoch is nontrivial, and boundary layer influence and source regions (see Figure S4) vary from season to season in such a way that it is plausible that the cloud processing effect is masked in Figure 4a. In summer, the out-of-cloud size distribution shows significantly higher concentrations. This is most likely explained by a strong PBL influence during sunny, warm periods. Wet deposition and in-cloud scavenging may play a role in forming this difference, too, but these effects are impossible to distinguish from transport processes from the PBL. The in-cloud case shows a more prominent Hoppel minimum [*Hoppel et al*., 1986] than the out-of-cloud situation, suggesting in-droplet heterogeneous production of secondary aerosol matter. However, the data do not actually allow us to exclude the possibility that cloudy conditions are preferentially connected to certain air mass origins and thus certain size distribution types (also see section 3.4). For autumn, Aitken mode particles are of about the same size for both conditions, with concentration differences of the same magnitude as in spring with the same possible causes. As pointed out above, autumn shows a distinct nucleation mode when the site is not inside the clouds. The accumulation mode number concentration differences in autumn are small, with somewhat more particles for out-of-cloud conditions and the mode shifted to larger size for in-cloud conditions (roughly from 120 to 130 nm in diameter). Compared to spring, the out-of-cloud accumulation mode particles are some 10 nm smaller in diameter, while the in-cloud accumulation mode is roughly at the same location resulting in in-cloud

concentrations above out-of-cloud concentrations for particles larger than about 130 nm diameter. This observation suggests that out-of-cloud accumulation mode particles in autumn experience, on average, less cloud processing than their spring counterparts, indicating differences in air mass history between the seasons which in turn points toward the influence of prevailing weather types on particle size distributions. The winter size distributions show generally low concentrations with higher concentrations for out-of-cloud conditions. Winter shows a nucleation mode when Jungfraujoch is cloud-free. The accumulation mode particles have roughly the same size for both situations. In contrast to autumn and spring, the winter accumulation mode shows significantly lower concentrations for in-cloud conditions. As E. Stopelli et al. (Ice nucleation active particles are efficiently removed by precipitating clouds, submitted to Scientific Reports, 2015) found, winter clouds have often experienced precipitation before they arrive at Jungfraujoch, which is also intuitively clear: during winter, clouds are formed well below Jungfraujoch altitude and have thus ample time for precipitation before reaching the site. This would deplete the accumulation mode which is consistent with our findings. In contrast, wet removal cannot be observed in a similarly clear way during spring and autumn. The most likely explanation for this is the "mixed nature" of those seasons, which contain both winter and summer characteristics. A significant part of the cloud-free situations during spring and autumn is connected to free tropospheric conditions (see section 3.3) which means lower concentrations in the Aitken and the accumulation mode. During May, on the other hand, the situation is likely to be summer-like. Clouds are connected with rising air masses meaning influences from lower altitudes and thus higher concentrations than found in the free troposphere. Wet deposition and other cloud-related removal processes are likely to occur, but the complex transport processes to Jungfraujoch and the varying degree of PBL influence mask their effect in Figure 4 for most seasons. Only in winter they can be clearly seen because boundary layer influences play only a minor role and the overall situation is thus less complex.

3.3. Free Troposphere and Boundary Layer Influence: Comparison of Various Approaches

We grouped the aerosol size distributions using the FLEXPART results in the form of the derived parameter "time since last significant boundary layer contact" (section 2.4). Figure 5 shows the median size distributions for the times specified in each panel's headline as well as the respective quartiles. The number of data points used for each panel is also indicated. Most noticeably, the vast majority (over 70%) of air masses arriving at Jungfraujoch had contact with the PBL within the last 24 h before arrival, followed by 18% without significant contact for at least 120 h before arrival. Only 5% and 3% of air masses had a last significant PBL contact between 24–48 h and 48–120 h before arrival. The fact that PBL influence happened either within the last 24 h or longer than 5 days ago in almost 90% of the cases indicates that the free troposphere is for the most part decoupled from the PBL on a larger spatial scale, except for the Alpine region around the Jungfraujoch (within 1 day horizontal transport), where orographically and thermally driven injections of PBL air are rather frequent.

We note a steady decline in the accumulation mode concentration with increasing time since last PBL contact. For the nucleation and Aitken modes, the situation is more complex. The median of the Aitken mode concentration stays about constant up to 72 h since the last PBL contact and only then decreases in the same way as the accumulation mode concentration. The upper quartile of the Aitken mode concentration, however, increases substantially, and between 48 and 96 h even shows a nucleation mode. As these high Aitken mode concentrations are not accompanied by equally high accumulation mode concentrations, we conclude that these particles were formed in the lower free troposphere. Apparently, a residence time of between 48 and 96 h in the lower free troposphere before arrival at Jungfraujoch results in the highest nucleation and Aitken mode concentrations. On one hand, this suggests that this is the time required to produce condensable vapors followed by new particle formation, growth, and transport (see Figure S5 for Aitken mode longevity) such that they are detected by our instrumentation. On the other hand, this effect may be enhanced by source areas providing suitable precursors for aerosol formation. For these observations, southerly advection often prevailed and the last PBL contact typically happened in Mediterranean regions, over Italy and Greece.

As mentioned above, the accumulation mode declines with time since the last PBL contact. To assess this process quantitatively, we show N_{90} (median and quartiles) as a function of time since the last PBL contact in Figure 6a. N_{90} and the accumulation mode number concentration are closely related, but we use N_{90} here because it is the most relevant number: as already stated above, 90 nm is the average threshold dry diameter above which particles are activated to cloud droplets when clouds form at Jungfraujoch [*Hammer et al.*, 2014].

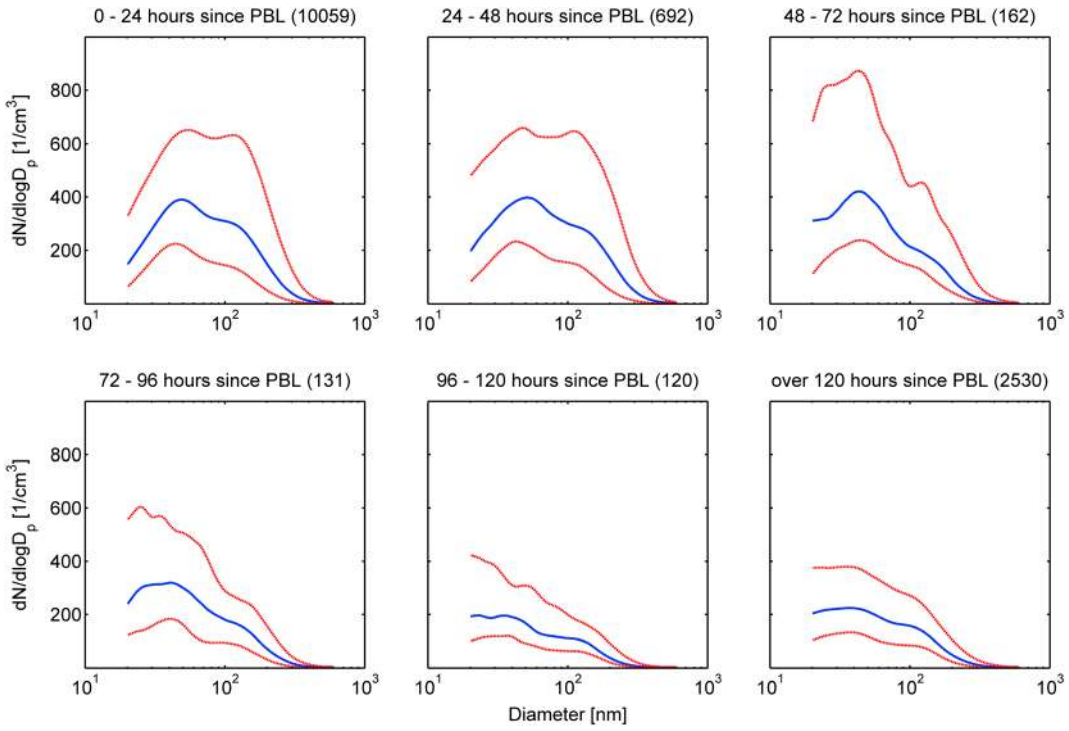

Figure 5. Median size distributions (blue) and respective quartiles (red) using the time elapsed since the last significant PBL contact as the grouping parameter. The number of data points is given in brackets.

Moreover, aerosol processes are related to the actual particle size while mode fitting is a descriptive tool. In Figure 6, we fitted the following function to the data:

$$N_{90} = C_0 + C_{\mathrm{inj}} \cdot \exp\left(C_{\mathrm{decay}} \cdot X\right) \tag{2}$$

While interpretations of some variables vary, the equation in this general form applies to Figures 6a and 6b and Figure S3. In all cases, C_0 denotes the N_{90} background concentration and C_{inj} is the median magnitude of the PBL injection. X is the x axis variable, i.e., time for the case time since PBL contact in Figure 6a. C_{decay}, finally, is the respective rate with which N_{90} approaches C_0.

With the coefficient of determination $R^2 = 0.9$ and also confirmed by Figure 6a, a good fit is possible. For time since PBL contact in Figure 6a, we find $C_{\mathrm{decay}} = -0.025$ which translates into a half-life of the N_{90} concentration of roughly 30 h to reach background conditions. For the background concentration C_0 of N_{90} in the FT we find $N_{90,\mathrm{background}} = 39\,\mathrm{cm}^{-3}$, and the typical magnitude of PBL injections over C_0 is $150\,\mathrm{cm}^{-3}$ for particles larger than 90 nm.

Figure 6b shows the same approach for the NO_y/CO case. This ratio has been used previously as a measure for FT conditions and PBL influence since NO_y/CO has been found to be a means of estimating the "age" of an air mass, with ratios of 0.1 to 0.16 (i.e., CO/NO_y between 6.25 and 10) close to anthropogenic sources and ratios of <0.01 (i.e., CO/$NO_y > 100$) after a few days of transport [*Jaeglé et al.*, 1998; *Stohl et al.*, 2002]. *Zellweger et al.* [2003] reported NO_y/CO ratios of 0.002 to 0.005 (i.e., CO/NO_y between 200 and 500) for free tropospheric conditions at Jungfraujoch depending on the season. The scatterplot of N_{90} versus CO/NO_y reveals a picture similar to the approach with simulated time since PBL contact and an analogous fit as described by equation (2) is possible. Of course, there is no time dependence in this case but the parameter C_0 remains the FT background concentration of N_{90}. With an R^2 of 0.99, the fit yields $C_0 = 46\,\mathrm{cm}^{-3}$. This is reasonably close to the value of $39\,\mathrm{cm}^{-3}$ from Figure 6a, which suggests that both approaches do indeed provide a similar quantitative assessment of free tropospheric conditions and boundary layer influence on N_{90} at Jungfraujoch.

Besides the medians and quartiles, Figures 6a and 6b also show the medians for summer and winter. Their C_0 values are very close to the respective upper and lower quartiles, which, of course, is no coincidence: Summer

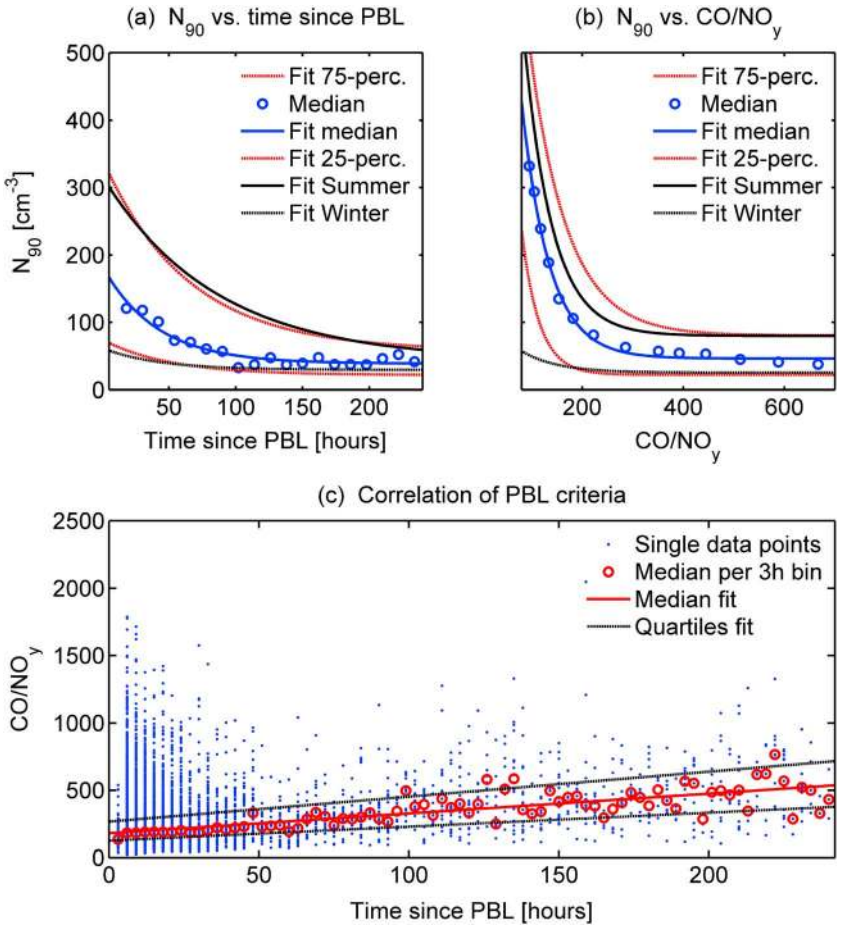

Figure 6. N_{90} (a) as a function of time since PBL and (b) as a function of CO/NO_y with fitted lines for median and quartiles. (c) The relation between time since PBL contact and CO/NO_y as well as the median values for each 3 h bin and a fit through them.

makes up one quarter of the year and has the strongest PBL influence; the same in reverse is true for winter. This suggests seasonality in N_{90} background in the lower free troposphere, which can be easily explained: as described in section 3.5, very little N_{90} is produced at Jungfraujoch. Injections from the PBL and transport from lower altitudes are thus the main sources for the observed N_{90}. The N_{90} background is therefore, essentially, an equilibrium between transport from below and dilution and loss processes, which will depend, among other things, on the frequency and strength of the injections. As there is more and stronger transport to Jungfraujoch during summer, those months will see higher background N_{90} concentrations. The loss processes, e.g., wet removal, may also have seasonality; however, it is not known whether they weaken or strengthen the seasonality of the N_{90} background value. For similar reasons, N_{90} background values will change somewhat each year, depending on prevalence of specific weather conditions.

To test whether the agreement between these approaches is merely coincidental, Figure 6c shows a plot of CO/NO_y versus time since the last PBL contact. With a 3 h time resolution for 10 days' back trajectories, the time since the last PBL contact is divided into 80 bins, and within each bin, there is a wide scatter of CO/NO_y values, especially for smaller CO/NO_y values and shorter time intervals since the last PBL contact. However, the median CO/NO_y values for each bin, denoted by red circles, show a solid linear correlation with time since PBL contact. This suggests that a good degree of similarity between results from both approaches can be expected; the consistent values for the background value of N_{90} are an example of this. The fact that the linear fit does not go through (0, 0) is a consequence of the nature of CO/NO_y. As pointed out above, this ratio is between 6.25 and 10 at the source and grows with air mass age. The offset of the fit from (0, 0) can thus be seen as a measure of the minimum distance from anthropogenic sources or the minimum age of air masses arriving at Jungfraujoch.

Another alternative to determine FT conditions and PBL influence are radon-222 concentrations, which are also available for Jungfraujoch, however, only for a shorter period of time (November 2009 to December 2012). Using similar reasoning as in Figure 6b, one can again plot N_{90} against 1/[^{222}Rn] and perform a similar fit (equation (2)). The resulting figure is very similar to Figures 6a and 6b and is shown for completeness in the supplement as Figure S3. For the FT background of N_{90} concentrations, the fit yields a value of 36.5 cm^{-3}, once again very much in line with the other two approaches.

Summarizing the three methods to discern FT conditions at Jungfraujoch, we find that $N_{90} = 40$ cm^{-3} is a good approximation to describe the free tropospheric background aerosol. This implies that N_{90} could be used as an additional criterion to identify FT conditions and to quantify the intensity of the PBL influence: the smaller the excess N_{90} above 40 cm^{-3} the less significant is the PBL influence. As stated above, this is an average value which differs between seasons (roughly 30 cm^{-3} in winter and 55 cm^{-3} in summer); however, this seasonality simply reflects a generally higher "residual PBL influence" in the warmer season with stronger convection. It is important to stress that the data do not suggest a sharp boundary between FT and PBL. Speaking instead of a varying degree of boundary layer influence reflects the observations more accurately.

It can nevertheless be instructive to derive FT limits from the fitted trend lines in Figures 6a and 6b and Figure S3 and to apply these limits in order to determine further similarities and differences between the respective approaches. To do this in a consistent manner, we define as "FT-like" situations where N_{90} exceeds the 40 cm^{-3} background concentration by a maximum of 50%. We then use the fitted equations and find the following limits: time since last contact with PBL = 78 h, CO/NO$_y$ = 260, and 1/[^{222}Rn] = 1.5 m^3 Bq^{-1}, which is equivalent to a radon-222 concentration of 0.67 Bq m^{-3}.

Figures 7a and 7b show the median size distributions for FT and PBL influence conditions assuming the three limits derived above to be sharp boundaries for free troposphere conditions. The legends in both figures also provide information about the prevalence of FT conditions. While the median distributions appear quite similar especially for the FT case, the percentage for FT conditions varies between 20 and 39% for the back trajectory and the CO/NO$_y$ approaches, respectively. Clearly, the analysis by CO/NO$_y$ ratio results in the least stringent FT criterion. The fact that the three median FT size distributions are almost identical indicates that the three criteria chose different subsets of data from the available, quite similar FT-like size distributions. In turn, the back trajectory and the ^{222}Rn criteria classify part of these as not FT, which leads to significantly lower concentrations for these criteria in the PBL-influenced data (Figure 7a). On average, the more stringent criteria exclude many FT-like size distributions while the less stringent CO/NO$_y$ criterion does not seem to classify significant numbers of PBL-type distributions as FT, which would lead to a markedly different median distribution in Figure 7b. With respect to the aerosol size distribution this would suggest that the least stringent of the applied criteria is the most accurate one. To make the back trajectory criterion less stringent it would, in principle, be possible to change the threshold for significant PBL contact (see section 2.2). However, tests have shown that already a small increase in the threshold value will increase the median size distribution in Figure 7b, i.e., PBL-type size distributions will be classified as FT. The attempt to change the ^{222}Rn threshold has similar consequences, indicating that local radon emissions as well as the comparatively long radon lifetime blur the distinction between free tropospheric conditions and boundary layer influence. This further supports the conclusion that the CO/NO$_y$ approach offers the best distinction between free troposphere conditions and boundary layer influence.

Figure 7c takes a closer look at the prevalence of FT conditions according to the three criteria throughout the year. As can be expected, all criteria find FT conditions to be more prevalent in winter than in summer. At all times, the FT percentage is lowest according to the time since PBL approach and highest according to CO/NO$_y$. The ^{222}Rn criterion approaches CO/NO$_y$ in summer and is close to the back trajectory approach in winter. Following the CO/NO$_y$ criterion, FT prevalence is around 20% in the summer and can be higher than 50% during autumn, winter, and spring, reaching over 60% in January. Notably, this gives a PBL influence for 40% of the time even during winter. This seems in contradiction to the winter panel of Figure 2 whose almost flat diurnal N_{90} curve suggests very little PBL influence during the winter. One has to remember, however, that these hard limits cannot account for varying degrees of PBL influence. As such, the figures are not contradicting each other but provide different aspects of PBL influence: Figure 2 describes the degree while Figure 7c shows the frequency.

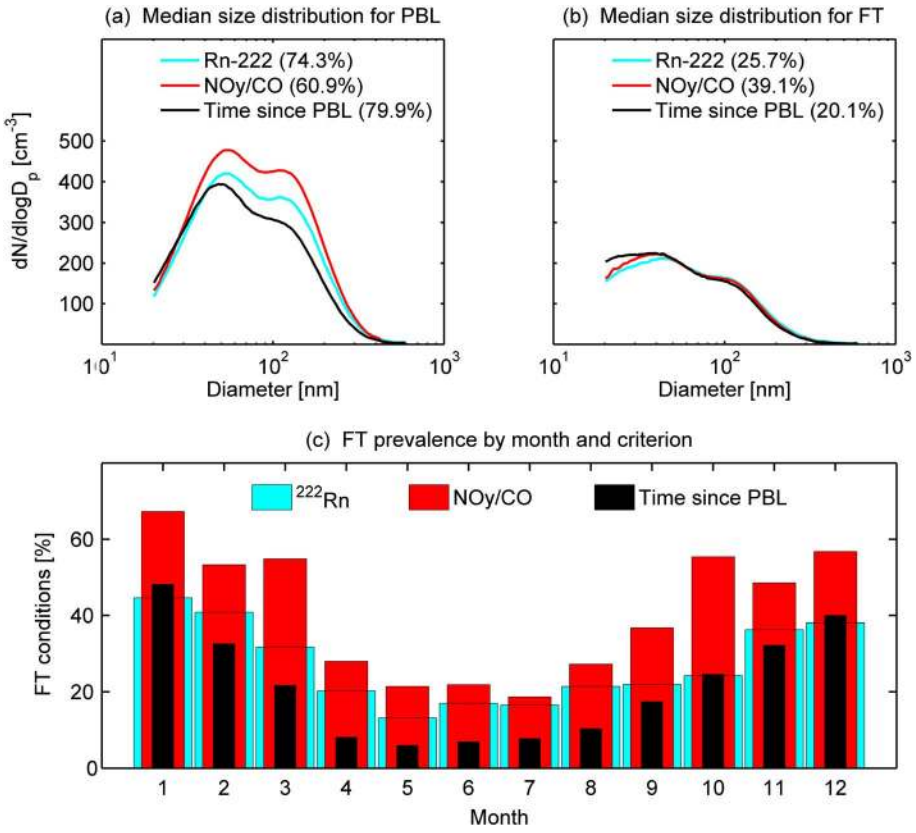

Figure 7. Median size distributions for (a) PBL and (b) FT conditions according to the three criteria. Numbers in brackets denote the retrieved frequencies of occurrence for the different selection approaches. (c) Relative occurrence of FT conditions at Jungfraujoch.

Finally, it is instructive to compare the newly derived FT criterion to the one applied in the previous Jungfraujoch size distribution study. In an approach adapted from Mauna Loa [*Mendonca and Iwaoka*, 1969], *Weingartner et al*. [1999] simply assumed that the site is in the free troposphere during the night, i.e., from 3:00 to 9:00 o'clock A.M. For this period, the CO/NO_y limit yields an FT percentage of only 46%. Of all situations that CO/NO_y identifies as free tropospheric merely 30% fall into the window between 3:00 and 9:00. In the light of our findings the assumption that nighttime equals FT conditions appears to miss most FT situations while also misclassifying a large amount of periods with boundary layer influence.

3.4. Air Mass Transport to Jungfraujoch

Surface source receptor relationships (SRRs; see section 2.4) were categorized following the clustering method described in *Sturm et al*. [2013] and *Pandey Deolal et al*. [2014] but applied here to the period January 2008 to May 2014. A separation into 12 categories was derived. The average relative surface SRRs (difference between the mean SRR of each category and the overall mean SRR, divided by the overall mean SRR) for these categories are given in Figure 8. The categories can be named following their main region of influence and the intensity of surface influence: (1) free tropospheric, (2) Alpine, (3) Central, (4) North-West strong, (5) North-West weak, (6) North-East, (7) East, (8) far South-East, (9) South, (10) South-West, (11) West weak, and (12) West strong.

Collaud Coen et al. [2011] used synoptic weather types [*Schüepp*, 1979] to describe transport of air masses to Jungfraujoch. *Wuesthoff* [2011] introduced new weather classification schemes which cannot be mapped onto the old approach and thus preclude a comparison with the *Collaud Coen et al*.'s [2011] results. Also, air mass classification on the basis of footprint clustering for a specific observational site (section 2.2 and Figure 8) seems more instructive than the weather-type approach. That is why we decided to use footprint clustering in this work, which has the added benefit of improving the time resolution from 1 day to 3 h.

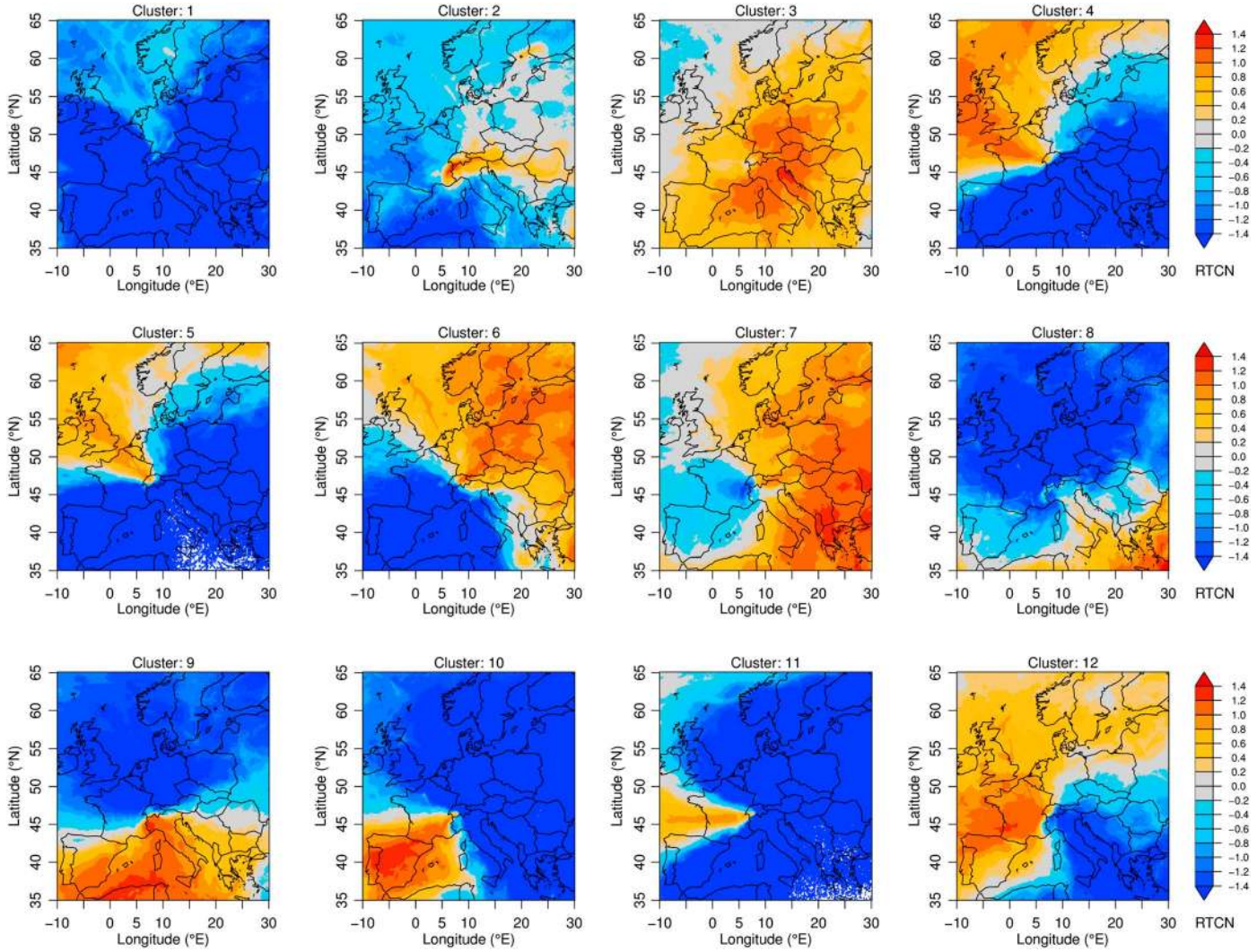

Figure 8. The 12 footprint clusters derived from FLEXPART calculations: (1) free tropospheric, (2) Alpine, (3) Central, (4) North-West strong, (5) North-West weak, (6) North-East, (7) East, (8) far South-East, (9) South, (10) South-West, (11) West weak, and (12) West strong. Plots are color-coded according to average relative surface SSR (source receptor relationships; see section 2.4) here expressed as residence times by cluster normalized (RTCN).

Figure 9 shows median distributions for each footprint cluster as well as quartiles and relative occurrence of each cluster where the occurrence varies between 5 and 11%. The figure also indicates which percentage of each cluster would be classified as free tropospheric according to the CO/NO_y criterion from section 3.3. Cluster 1 ("free tropospheric") produces a median size distribution that is quite similar to the distributions that the different FT criteria yield in Figure 7b. Consistent with this observation, 68% of this cluster would be classified as FT with the CO/NO_y criterion. However, with an occurrence of 9.6%, it is well below even the strictest FT criterion in the section above and much lower than the suggested FT frequency of 39%. Instances of cluster 1 air masses are distributed throughout the year very much like FT conditions as the comparison of Figure 7c and Figure S4 shows. Cluster 2 ("Alpine") covers nearby regions which correspond to recent PBL injections and thus relatively high concentrations. Clusters 4 ("North-West strong") and 5 ("North-West weak") appear to be very similar in Figure 8 and also produce very similar size distributions in Figure 9. Only the Aitken mode for cluster 4 seems slightly more prominent. Cluster 8 shows surface contributions mainly quite far away over the South-East Mediterranean where these air masses were not altered by significant PBL contact during their further approach to Jungfraujoch. With the time since last PBL contact criterion, a significant part of this cluster would be classified as FT, and the CO/NO_y criterion gives an FT fraction of 52%. Also, its monthly frequency distribution (Figure S4) resembles the annual distribution of FT conditions (Figure 7c).

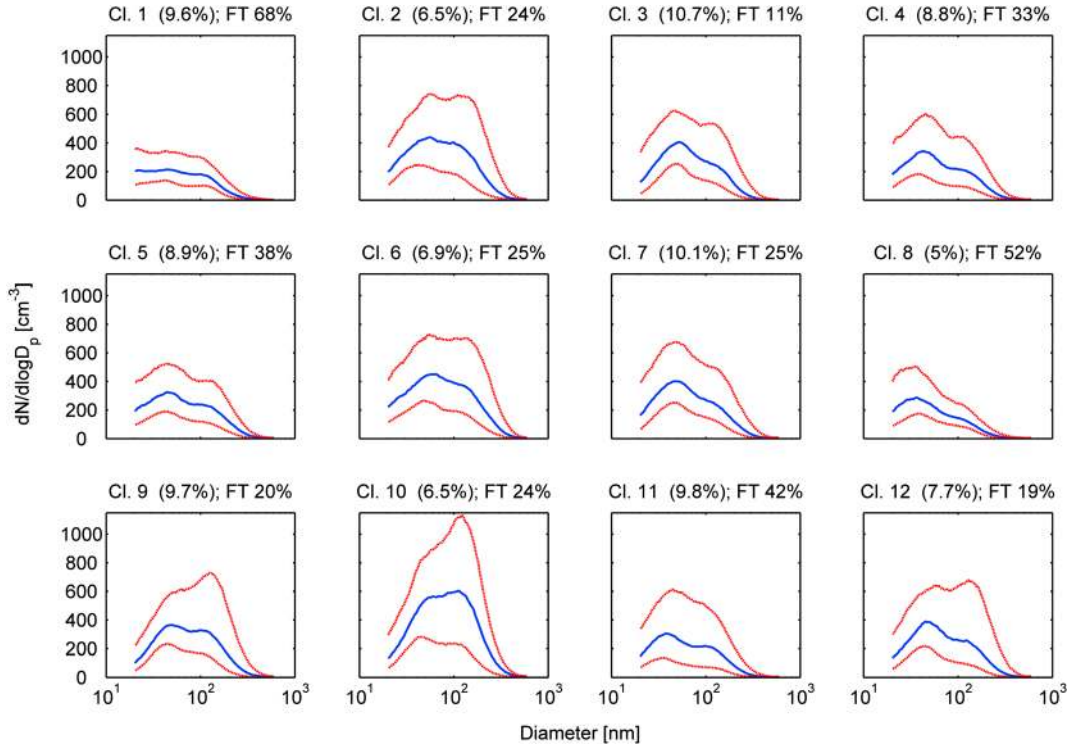

Figure 9. Median size distribution for footprint clusters (medians in blue, quartiles in red). Prevalence is given with each figure. The free troposphere percentage indicates which fraction of each cluster fulfils the CO/NO_y FT criterion derived in section 3.3 and also applied in Figure 7. Clusters as in Figure 8: (1) free tropospheric, (2) Alpine, (3) Central, (4) North-West strong, (5) North-West weak, (6) North-East, (7) East, (8) far South-East, (9) South, (10) South-West, (11) West weak, and (12) West strong.

However, the prominent Aitken mode suggests that cluster 8 is not purely FT (compare to Figure 7b). In fact, the shape of the size distribution resembles the ones covering the time from 48 to 96 h in Figure 5. Such short residence time in the FT will hardly be enough to remove all recent PBL influence. The largest accumulation mode is connected to cluster 10 where it shows especially in the upper quartile. Comparing this to Figure 4 suggests that this is connected to cloud-free conditions in summer. Consistently, cluster 10 frequency is highest in summer (Figure S4). Of the remaining clusters, cluster 6 ("North-East") shows the highest concentrations. This is the cluster that is most influenced by eastern Europe. The quite similar cluster 7 ("East"), which includes more air masses from South-East Europe, shows noticeably lower concentrations for both modes. Clusters 9 ("South") and 12 ("West strong") show frequent transport from the PBL as the large accumulation modes in the upper quartiles indicate. Finally, cluster 3 shows the lowest free troposphere percentage of all clusters. This does not, however, result in the highest particle concentrations—a good reminder that boundary layer influence is a matter of degree and that the results of sharp FT limits should not be overinterpreted.

3.5. New Particle Formation, Growth, and In Situ CCN Production

A detailed analysis of the very first steps of particle formation is not possible based on size distributions measured between 20 and 600 nm and additional measurements of N_{10} alone. However, based on the observation of particle growth and the temporal evolution of N_{10-20} (the number concentration of particles with diameters between 10 and 20 nm), the frequency of recent new particle formation (NPF) events in the air masses arriving at Jungfraujoch can be estimated with reasonable accuracy. NPF events were identified by visual inspection of daily size distribution contour plots and additional N_{10-20} data. Identification and classification follow the protocol outlined by *Kulmala et al.* [2012]. Days were classified as event days (Class 1 or Class 2), undefined days, or nonevent days, depending on appearance of small particles, observable particle growth, event intensity, and event duration.

Table 2. Frequency of New Particle Formation Events Throughout the Year

	Class 1 Events (%)	All Events (%)	Undefined (%)	Nonevents (%)
January	5.1	13.1	3.6	83.2
February	4.5	16.0	5.8	78.2
March	8.3	27.2	5.3	67.5
April	9.3	18.6	8.7	72.7
May	4.6	11.6	5.8	82.7
June	2.0	9.2	3.9	86.9
July	3.4	12.4	4.0	83.6
August	3.5	14.0	6.4	79.5
September	3.9	10.8	2.9	86.3
October	5.9	16.0	5.9	78.2
November	4.1	9.3	6.2	84.5
December	2.7	11.5	5.3	83.2
All 6 years	4.9	14.5	5.4	80.1

Table 2 shows the nucleation frequency for each month. It is highest in March and April but there is no distinct annual pattern and year-to-year variation is large. Over the whole period of 6 years, new particle formation was observed on 14.5% of days. This is somewhat below the 17.5% *Boulon et al.* [2010] reported for 1 year of observations at Jungfraujoch. In their study, they used a neutral cluster and air ion spectrometer (NAIS), which measures neutral clusters as small as 2 nm and detects ions with 0.8 nm diameter. This means that *Boulon et al.* [2010] were able to detect events that could not be observed with a lower cutoff diameter of 10 nm as in this study; a somewhat higher nucleation frequency has thus to be expected. Compared to other high-altitude sites, new particle formation at Jungfraujoch occurs rather infrequently. For example, at Chacaltaya in Bolivia, *Rose et al.* [2015] observed nucleation almost on a daily basis during the local dry season. For Storm Peak in Colorado, *Hallar et al.* [2011] have reported a nucleation frequency of 52%. *García et al.* [2014] found 30% in their long-term study at Izaña, and *Boulon et al.* [2011] 36% for Puy de Dôme. As an outlier in the global observations, *Neitola et al.* [2011] have reported nucleation probabilities for Mukteshwar that are as low as the ones found at Jungfraujoch. But in contrast to our findings, Mukteshwar shows a very pronounced annual cycle.

Table 2 separately lists Class 1 events which are characterized by a large increase in $N_{10–20}$ and continued growth over several hours. These very strong and distinct events occur only once or twice per month. Their clear features, however, allow for a closer inspection of their characteristics. New particle formation starts earlier in summer than in winter, as also shown in Figure 2, as expected by the earlier sunrise. From the time that passes between the onset of the concentration increase in N_{10} and N_{20}, it is possible to estimate the growth rate between these diameters. Typically, N_{10} and N_{20} increases are shifted by 1 to 2 h. This implies an upper limit for the mean growth rate of about 6 nm h^{-1} which is close to the value of 5.7 for growth from 7 to 20 nm found by *Boulon et al.* [2010]. Considering growth rates at elevated sites, in general, one notices very heterogeneous results. Some locations are reported to show small growth rates around 0.5 nm h^{-1} (Izaña [*García et al.*, 2014] and Mauna Loa [*Weber et al.*, 1995]). A number of sites have been found to have growth rates around 2.5 nm h^{-1} (Norikura [*Nishita et al.*, 2008], Mukteshwar [*Neitola et al.*, 2011], and Dome C [*Järvinen et al.*, 2013]). Values close to the 6 nm h^{-1} observed at Jungfraujoch have been reported for Puy de Dôme [*Boulon et al.*, 2011], Chacaltaya [*Rose et al.*, 2015], and Storm Peak [*Hallar et al.*, 2011].

Based on the evolution of $N_{10–20}$ over time it is further possible to estimate an "apparent formation rate" (the maximum slope of $N_{10–20}$ over time) of these particles, which is about 1 cm^{-3} s^{-1} on average but the determination of an actual nucleation rate requires too many assumptions to be reliable. For comparison, formation rates in the literature reach from 0.023 cm^{-3} s^{-1} (Dome C [*Järvinen et al.*, 2013]) to 7.47 cm^{-3} s^{-1} (Storm Peak [*Hallar et al.*, 2011]). $N_{10–20}$ typically peaks at 3000 cm^{-3} (median) on event days, while values of over 15000 cm^{-3} are observed during the strongest events. In contrast to this, $N_{10–20}$ typically does not exceed 500 cm^{-3} on nonevent days.

While particle formation rates and initial growth below 20 nm can only be approximated, the available data permit a clear look at subsequent particle growth eventually resulting in CCN formation, i.e., growth to 90 nm and beyond. Above 20 nm, the growth rate rapidly declines. Newly formed particles typically do not grow beyond the Aitken mode, with the biggest particles reaching 60 or 70 nm as evident from surface plots (Figure S5). In 6 years, no event was observed in which newly formed particles continued to grow to CCN sizes in significant numbers within the same air mass which means within 1 or 2 days. This is in contrast to observations by *Pierce et al.* [2012] who found significant CCN production driven by biogenic organic compounds following nucleation events on Whistler Mountain. One has to point out, however, that the two sites on Whistler Mountain are at 1300 m and 2182 m asl, while Jungfraujoch is at 3580 m and well removed from biogenic sources. In some

cases, preexisting particles of the Aitken mode grew to larger sizes during new particle formation events, i.e., when much condensable vapor was available. However, such growth of the Aitken mode is quite rare, of all Class 1 events, only some 20 cases with notable increase in CCN concentration were identified in the 6 year data set while Class 2 events typically do not contribute to CCN numbers. When this occurs, the CCN yield is significant with an average of 100 cm^{-3}. However, one has to keep in mind that this value is only an upper limit since part of the increase in N_{90} is likely connected to PBL influence which is typical for nucleation days. The contribution of this process to average CCN concentrations at Jungfraujoch is only roughly 1 CCN cm^{-3} d^{-1} on average, i.e., on the order of magnitude of 1%. In the light of these numbers it is justified to conclude that the greatest fraction of CCN at Jungfraujoch originates from the boundary layer or was formed during the vertical transport of air masses to Jungfraujoch. However, this does not exclude that new particles formed in the FT eventually end up as CCN. They can possibly be mixed down to the PBL, where growth to CCN sizes is more efficient due to higher concentration of condensable vapors. However, the fact that in situ CCN formation in the FT is negligible compared to vertical transport of CCN to the Jungfraujoch is an essential observation that validates the approach of using the number concentration of accumulation mode particles in the determination of a criterion for FT conditions as described in section 3.3.

4. Summary and Conclusions

The aerosol size distribution at Jungfraujoch was measured over a period of 6 years with an SMPS system covering the particle diameters between 20 and 600 nm. Additional data include the total particle number concentration above 10 nm, long-wave radiation, ambient temperature, relative humidity, NO_y, CO, and ^{222}Rn concentrations. FLEXPART simulations provided information on the history of the sampled air masses.

N_{10} shows a clear diurnal cycle for all seasons. During summer, daily variability is driven by PBL influence which affects nucleation, Aitken, and accumulation modes while daily variations of Aitken and accumulation mode concentrations are very small in winter. $N_{10–20}$ shows a distinct diurnal cycle throughout the whole year, implicating that new particle formation occurs in all seasons. As can be expected, nucleation starts earliest during the day in summer and latest in winter. New particle formation has been observed on 14.5% of all days with highest values in spring but without a clear seasonal pattern and high year-to-year variation. New particles grow relatively fast from 10 to 20 nm (6 nm h^{-1} for Class 1 events) but do not grow beyond Aitken mode sizes. The growth of new particles all the way to CCN sizes within 2 days of nucleation onset has not been observed. Occasionally, preexisting Aitken mode particles grow above 90 nm during nucleation events but the process is rare and contributes very little to average CCN concentrations. Ultimately, CCN concentrations at Jungfraujoch are thus almost exclusively driven by transport from lower altitudes.

The sky temperature, which can be calculated from long-wave radiation, has been used as a parameter to determine cloud presence. To verify this approach, it was compared to automated analysis of webcam photos taken at 1 h intervals. Both approaches show very good agreement indicating that the sky temperature is a reliable parameter to identify cloud presence in the absence of direct in situ cloud measurements. RH as a cloud proxy works poorly in comparison at this location.

Three parameters were used to identify free tropospheric conditions and the influence of the planetary boundary layer. Based on FLEXPART simulations we developed the parameter "time since PBL contact," which is the time that has passed since the air mass had the last significant contact with the boundary layer. For comparison, also CO/NO_y (as a derivation of the previously used NO_y/CO) and ^{222}Rn concentrations were used to determine PBL influence. Combining these approaches, we found that the tropospheric background concentration of N_{90} (≈CCN) is about 40 cm^{-3} at the site with a certain amount of variation throughout the year. As N_{90} at Jungfraujoch is almost exclusively originating from lower altitudes, this annual variation is easily explained by the varying frequency of transport to Jungfraujoch, which is a consequence of varying temperature and day length. The value of 40 cm^{-3} is derived in such a way that it does not constitute a threshold between FT and PBL situations but a value toward which N_{90} will develop given that there are no fresh injections from below. By the same token, time since PBL, CO/NO_y, and ^{222}Rn does not provide sharp FT thresholds. Nevertheless, limits can be derived that describe "almost background" conditions. Using these as FT limits, we can determine the shape of the average FT size distribution and find that FT conditions prevail for 39% of the time, ranging from around 20% in summer to over 60% in January. It is noteworthy that even during winter, Jungfraujoch is not at all times in the free troposphere.

Compared to other high-altitude sites, new particle formation at Jungfraujoch is rare and shows no clear annual cycle. While such scarcity renders a detailed statistical analysis of NPF at Jungfraujoch quite challenging in terms of the required time series, it also provides an opportunity to determine the conditions that favor nucleation at high altitude: contrasting NPF conditions and conditions where no NPF occurs is a powerful tool to this end. Closely related to this challenge is the observation that newly formed particles do not grow to CCN size immediately while nucleation in the PBL is often related to large CCN gains [e.g., *Herrmann et al.*, 2014]. This leads to the question at which height CCN are still produced. Jungfraujoch and the surrounding region with its infrastructure and the resulting easy access provide the ideal ambient laboratory to study nucleation, CCN formation, and the necessary conditions at various altitudes.

In closing, the lower free troposphere at Jungfraujoch is strongly influenced by injections from the planetary boundary layer and other transport processes from lower altitudes. Seventy percent of the air masses arriving at the site had boundary layer contact within the last 24 h before arrival, and almost 20% had no significant PBL influence during the previous 5 days. This bimodal distribution suggests that vertical transport happens mainly in (and is likely caused by) the Alps, while it happens only infrequently over nonmountainous regions. With the mountains as a main factor for vertical transport, one would expect that the PBL influence depends on the characteristics of the mountain(s) in questions. Twenty-seven percent of the Earth's land surface is defined as mountainous (altitude $>$ 1500 m asl) [*Messerli and Ives*, 1997]. The currently best climate models have a resolution of 25 km [*Wehner et al.*, 2014] and thus cannot capture accurately PBL influence on the free troposphere driven by orographic effects over a significant portion of the globe's surface. While model studies [e.g., *Spracklen et al.*, 2010] show reasonable agreement between observed and modeled number concentrations at sites such as Jungfraujoch, our findings suggest that further improvement requires a finer resolution of the transport processes from the boundary layer to the free troposphere especially over mountain areas.

Acknowledgments

We thank the International Foundation High Altitude Research Stations Jungfraujoch and Gornergrat for the opportunity to perform experiments on the Jungfraujoch. Especially, we would like to thank the research station's custodians Joan and Martin Fischer, Maria and Urs Otz, and Susanne and Felix Seiler for their past and present support and hospitality. The Swiss National Air Pollution Monitoring Network is run by Empa in collaboration with the Swiss Federal Office for the Environment. This work was supported by MeteoSwiss in the framework of the Global Atmosphere Watch program, FP7 project ACTRIS (grant agreement 262254) and FP7 project BACCHUS (grant agreement 603445). M.G. was supported by the ERC (grant agreement 615922-BLACARAT). The SMPS data used in this work have been submitted to EBAS and will be available for download at http://ebas.nilu.no. Radon data are available at http://azug.minpet.unibas.ch/~lukas/pl/radon.pl. Trace gas data are submitted annually to http://ds.data.jma.go.jp/gmd/wdcgg/. Meteorological data are available from MeteoSwiss. FLEXPART simulation results can be viewed at http://lagrange.empa.ch/FLEXPART_browser/. All data and results can be requested from the corresponding author at erik.herrmann@psi.ch.

References

Baltensperger, U., H. Gäggeler, D. Jost, M. Lugauer, M. Schwikowski, E. Weingartner, and P. Seibert (1997), Aerosol climatology at the high-alpine site Jungfraujoch, Switzerland, *J. Geophys. Res.*, *102*, 19,707–19,715, doi:10.1029/97JD00928.

Baltensperger, U., M. Schwikowski, D. T. Jost, S. Nyeki, H. W. Gäggeler, and O. Poulida (1998), Scavenging of atmospheric constituents in mixed phase clouds at the high-alpine site Jungfraujoch Part I: Basic concept and aerosol scavenging by clouds, *Atmos. Environ.*, *32*(23), 3975–3983, doi:10.1016/S1352-2310(98)00051-X.

Balzani Lööv, J. M., S. Henne, G. Legreid, J. Staehelin, S. Reimann, A. S. H. Prévôt, M. Steinbacher, and M. K. Vollmer (2008), Estimation of background concentrations of trace gases at the Swiss Alpine site Jungfraujoch (3580 m asl), *J. Geophys. Res.*, *113*, D22305, doi:10.1029/2007JD009751.

Baron, P., and K. Willeke (2005), *Aerosol Measurement: Principles, Techniques, and Applications*, Wiley-Interscience, New York.

Boulon, J., et al. (2010), New particle formation and ultrafine charged aerosol climatology at a high altitude site in the Alps (Jungfraujoch, 3580 m a.s.l., Switzerland), *Atmos. Chem. Phys.*, *10*, 9333–9349, doi:10.5194/acp-10-9333-2010.

Boulon, J., K. Sellegri, M. Hervo, D. Picard, J.-M. Pichon, P. Fréville, and P. Laj (2011), Investigation of nucleation events vertical extent: A long term study at two different altitude sites, *Atmos. Chem. Phys.*, *11*, 5625–5639, doi:10.5194/acp-11-5625-2011.

Brunner, D., S. Henne, C. A. Keller, S. Reimann, M. K. Vollmer, S. O'Doherty, and M. Maione (2012), An extended Kalman-filter for regional scale inverse emission estimation, *Atmos. Chem. Phys.*, *12*, 3455–3478, doi:10.5194/acp-12-3455-2012.

Clarke, A. D., J. L. Varner, F. Eisele, R. L. Maudin, D. Tanner, and M. Litchy (1998), Particle production in the remote marine atmosphere: Cloud outflow and subsidence during ACE-1, *J. Geophys. Res.*, *103*, 16,396–16,409, doi:10.1029/97JD02987.

Collaud Coen, M., E. Weingartner, D. Schaub, C. Hueglin, C. Corrigan, S. Henning, M. Schwikowski, and U. Baltensperger (2004), Saharan dust events at the Jungfraujoch: Detection by wavelength dependence of the single scattering albedo and first climatology analysis, *Atmos. Chem. Phys.*, *4*, 2465–2480, doi:10.5194/acp-4-2465-2004.

Collaud Coen, M., E. Weingartner, S. Nyeki, J. Cozic, S. Henning, B. Verheggen, R. Gehrig, and U. Baltensperger (2007), Long-term trend analysis of aerosol variables at the high-alpine site Jungfraujoch, *J. Geophys. Res.*, *112*, D13213, doi:10.1029/2006JD007995.

Collaud Coen, M., E. Weingartner, M. Furger, S. Nyeki, A. S. H. Prévôt, M. Steinbacher, and U. Baltensperger (2011), Aerosol climatology and planetary boundary influence at the Jungfraujoch analyzed by synoptic weather types, *Atmos. Chem. Phys.*, *11*, 5931–5944, doi:10.5194/acp-11-5931-2011.

Cozic, J., B. Verheggen, S. Mertes, P. Connolly, K. Bower, A. Petzold, U. Baltensperger, and E. Weingartner (2007), Scavenging of black carbon in mixed phase clouds at the high alpine site Jungfraujoch, *Atmos. Chem. Phys.*, *7*, 1797–1807, doi:10.5194/acp-7-1797-2007.

Ebert, M., A. Worringen, N. Benker, S. Mertes, E. Weingartner, and S. Weinbruch (2011), Chemical composition and mixing-state of ice residuals sampled within mixed phase clouds, *Atmos. Chem. Phys.*, *11*, 2805–2816, doi:10.5194/acp-11-2805-2011.

Fiebig, M., D. Hirdman, C. R. Lunder, J. A. Ogren, S. Solberg, A. Stohl, and R. L. Thompson (2014), Annual cycle of Antarctic baseline aerosol: Controlled by photooxidation-limited aerosol formation, *Atmos. Chem. Phys.*, *14*, 3083–3093, doi:10.5194/acp-14-3083-2014.

García, M. I., S. Rodríguez, Y. González, and R. D. García (2014), Climatology of new particle formation at Izaña mountain GAW observatory in the subtropical North Atlantic, *Atmos. Chem. Phys.*, *14*, 3865–3881, doi:10.5194/acp-14-3865-2014.

Griffiths, A. D., F. Conen, E. Weingartner, L. Zimmermann, S. D. Chambers, A. G. Williams, and M. Steinbacher (2014), Surface-to-mountaintop transport characterised by radon observations at the Jungfraujoch, *Atmos. Chem. Phys.*, *14*, 12,763–12,779, doi:10.5194/acp-14-12763-2014.

Gröbner, J., I. Reda, S. Wacker, S. Nyeki, K. Behrens, and J. Gorman (2014), A new absolute reference for atmospheric longwave irradiance measurements with traceability to SI units, *J. Geophys. Res. Atmos.*, *119*, 7083–7090, doi:10.1002/2014JD021630.

Hallar, A. G., D. H. Lowenthal, G. Chirokova, R. D. Borys, and C. Wiedinmyer (2011), Persistent daily new particle formation at a mountain-top location, *Atmos. Environ.*, *45*, 4111–4115, doi:10.1016/j.atmosenv.2011.04.044.

Hammer, E., N. Bukowiecki, M. Gysel, Z. Jurányi, C. R. Hoyle, R. Vogt, U. Baltensperger, and E. Weingartner (2014), Investigation of the effective peak supersaturation for liquid-phase clouds at the high-alpine site Jungfraujoch, Switzerland (3580 m a.s.l.), *Atmos. Chem. Phys.*, *14*, 1123–1139, doi:10.5194/acp-14-1123-2014.

Henne, S., D. Brunner, D. Folini, S. Solberg, J. Klausen, and B. Buchmann (2010), Assessment of parameters describing representativeness of air quality in-situ measurement sites, *Atmos. Chem. Phys.*, *10*, 3561–3581, doi:10.5194/acp-10-3561-2010.

Henning, S., E. Weingartner, S. Schmidt, M. Wendisch, H. W. Gäggeler, and U. Baltensperger (2002), Size-dependent aerosol activation at the high-alpine site Jungfraujoch (3580 m asl), *Tellus*, *54B*, 82–95.

Herrmann, E., et al. (2014), Aerosols and nucleation in eastern China: First insights from the new SORPES-NJU station, *Atmos. Chem. Phys.*, *14*, 2169–2183, doi:10.5194/acp-14-2169-2014.

Hoppel, W., G. Frick, and R. Larson (1986), Effect of nonprecipitating clouds on the aerosol size distribution in the marine boundary layer, *Geophys. Res. Lett.*, *13*, 125–128, doi:10.1029/GL013i002p00125.

Hussein, T., M. Dal Maso, T. Petäjä, I. K. Koponen, P. Paatero, P. P. Aalto, K. Hämeri, and M. Kulmala (2005), Evaluation of an automatic algorithm for fitting the particle number size distributions, *Boreal Environ. Res.*, *10*, 337–355.

Jaeglé, L., D. J. Jacob, Y. Wang, A. J. Weinheimer, B. A. Ridley, T. L. Campos, G. W. Sachse, and D. E. Hagen (1998), Sources and chemistry of NO_x in the upper troposphere over the United States, *Geophys. Res. Lett.*, *25*, 1705–1708, doi:10.1029/97GL03591.

Järvinen, E., et al. (2013), Seasonal cycle and modal structure of particle number size distribution at Dome C, Antarctica, *Atmos. Chem. Phys.*, *13*, 7473–7487, doi:10.5194/acp-13-7473-2013.

Jurányi, Z., M. Gysel, E. Weingartner, N. Bukowiecki, L. Kammermann, and U. Baltensperger (2011), A 17 month climatology of the cloud condensation nuclei number concentration at the high alpine site Jungfraujoch, *J. Geophys. Res.*, *116*, D10204, doi:10.1029/2010JD015199.

Kalivitis, N., G. Kouvarakis, A. Bougiatioti, I. Stavroulas, H. E. Manninen, M. Kulmala, V.-M. Kerminen, and N. Mihalopoulos (2015), Long-term observations of new particle formation in Eastern Mediterranean atmosphere, Geophys. Res. Abstracts, 17, EGU2015-12460.

Kamphus, M., M. Ettner-Mahl, T. Klimach, F. Drewnick, L. Keller, D. J. Cziczo, S. Mertes, S. Borrmann, and J. Curtius (2010), Chemical composition of ambient aerosol, ice residues and cloud droplet residues in mixed-phase clouds: Single particle analysis during the Cloud and Aerosol Characterization Experiment (CLACE 6), *Atmos. Chem. Phys.*, *10*, 8077–8095, doi:10.5194/acp-10-8077-2010.

Keller, C. A., et al. (2012), European emissions of halogenated greenhouse gases inferred from atmospheric measurements, *Environ. Sci. Technol.*, *46*, 217–225, doi:10.1021/es202453j.

Kipp & Zonen (2014), Instruction manual—CGR 4 pyrgeometer. [Available at http://www.kippzonen.com/Download/38/Manual-CGR-4-Pyrgeometer, accessed 04/12/2014.]

Korolev, A., and G. Isaac (2006), Relative humidity in liquid, mixed-phase, and ice clouds, *J. Atmos. Sci.*, *63*, 2865–2880, doi:10.1175/JAS3784.1.

Kulmala, M., et al. (2012), Measurement of the nucleation of atmospheric aerosol particles, *Nat. Protoc.*, *7*, 1651–1667, doi:10.1038/nprot.2012.091.

Lugauer, M., U. Baltensperger, M. Furger, H. W. Gaggeler, D. T. Jost, M. Schwikowski, and H. Wanner (1998), Aerosol transport to the high Alpine sites Jungfraujoch (3454 m a.s.l.) and Colle Gnifetti (4452 m a.s.l.), *Tellus B*, *50*, 76–92.

McArthur, L. J. B. (2005), Baseline Surface Radiation Network (BSRN) Operations Manual version 2.1, WCRP-121, WMO/TD-No. 1274.

Mendonca, B. G., and W. T. Iwaoka (1969), The trade wind inversion at the slopes of Mauna Loa, Hawaii, *J. Appl. Meteorol.*, *8*, 213–219, doi:10.1175/1520-0450(1969)008<0213:TTWIAT>2.0.CO;2.

Merikanto, J., D. V. Spracklen, G. W. Mann, S. J. Pickering, and K. S. Carslaw (2009), Impact of nucleation on global CCN, *Atmos. Chem. Phys.*, *9*, 8601–8616, doi:10.5194/acp-9-8601-2009.

Messerli, B., and J. Ives (Eds.) (1997), *Mountains of the World: A Global Priority*, Parthenon, New York & London.

Neitola, K., E. Asmi, M. Komppula, A.-P. Hyvärinen, T. Raatikainen, T. S. Panwar, V. P. Sharma, and H. Lihavainen (2011), New particle formation infrequently observed in Himalayan foothills—Why?, *Atmos. Chem. Phys.*, *11*, 8447–8458, doi:10.5194/acp-11-8447-2011.

Nieminen, T., A. Asmi, M. Dal Maso, P. P. Aalto, P. Keronen, T. Petäjä, M. Kulmala, and V.-M. Kerminen (2014), Trends in atmospheric new-particle formation: 16 years of observations in boreal forest environment, *Boreal Environ. Res.*, *19*(suppl. B), 191–214.

Nishita, C., K. Osada, M. Kido, K. Matsunaga, and Y. Iwasaka (2008), Nucleation mode particles in upslope valley winds at Mount Norikura, Japan: Implications for the vertical extent of new particle formation events in the lower troposphere, *J. Geophys. Res.*, *113*, D06202, doi:10.1029/2007JD009302.

Nyeki, S., U. Baltensperger, I. Colbeck, D. T. Jost, E. Weingartner, and H. W. Gäggeler (1998), The Jungfraujoch high-alpine research station (3454 m) as a background clean continental site for the measurement of aerosol parameters, *J. Geophys. Res.*, *103*(D6), 6097–6107, doi:10.1029/97JD03123.

Olivier, J. G. J., and J. J. M. Berdowski (2001), Global emissions sources and sinks, in *The Climate System*, edited by J. J. M. Berdowski, R. Guicherit, and J. B. Heij, A.A. Balkema Publishers/Swets & Zeitlinger Publishers, Lisse, Netherlands.

Pandey Deolal, S., D. Brunner, M. Steinbacher, U. Weers, and J. Staehelin (2012), Long-term in situ measurements of NO_x and NO_y at Jungfraujoch 1998–2009: Time series analysis and evaluation, *Atmos. Chem. Phys.*, *12*, 2551–2566, doi:10.5194/acp-12-2551-2012.

Pandey Deolal, S., J. Staehelin, D. Brunner, J. Cui, M. Steinbacher, C. Zellweger, S. Henne, and M. K. Vollmer (2013), Transport of PAN and NO_y from different source regions to the Swiss high alpine site Jungfraujoch, *Atmos. Environ.*, *64*, 103–115, doi:10.1016/j.atmosenv.2012.08.021.

Pandey Deolal, S., S. Henne, L. Ries, S. Gilge, U. Weers, M. Steinbacher, J. Staehelin, and T. Peter (2014), Analysis of elevated springtime levels of peroxyacetyl nitrate (PAN) at the high Alpine research sites Jungfraujoch and Zugspitze, *Atmos. Chem. Phys.*, *14*, 12,553–12,571, doi:10.5194/acp-14-12553-2014.

Philipona, R., A. Heimo, and B. Hoegger (1993), Investigations of solar radiation detectors using a laboratory test facility for solar radiation meteorological instruments, *Sol. Energy*, *51*(2), 159–163, doi:10.1016/0038-092X(93)90077-2.

Philipona, R., et al. (2001), Atmospheric longwave irradiance uncertainty: Pyrgeometers compared to an absolute sky-scanning radiometer, atmospheric emitted radiance interferometer, and radiative transfer model calculations, *J. Geophys. Res.*, *106*, 28,129–28,142, doi:10.1029/2000JD000196.

Pierce, J. R., et al. (2012), Nucleation and condensational growth to CCN sizes during a sustained pristine biogenic SOA event in a forested mountain valley, *Atmos. Chem. Phys.*, *12*, 3147–3163, doi:10.5194/acp-12-3147-2012.

Rose, C., K. Sellegri, F. Velarde, I. Moreno, M. Ramonet, K. Weinhold, R. Krejci, M. Andrade, A. Wiedensohler, and P. Laj (2015), Frequent nucleation events at the high altitude station of Chacaltaya (5240 m a.s.l.), Bolivia, *Atmos. Environ.*, *102*, 18–29, doi:10.1016/j.atmosenv.2014.11.015.

Schüepp, M. (1979), Witterungsklimatologie, Klimatologie der Schweiz, Band III, Beilage zu den Annalen 1978. [Available from MeteoSwiss, Zürich, Switzerland.]

Seibert, P., and A. Frank (2004), Source-receptor matrix calculation with a Lagrangian particle dispersion model in backward mode, *Atmos. Chem. Phys.*, *4*, 51–63, doi:10.5194/acp-4-51-2004.

Seinfeld, J. H., and S. N. Pandis (2006), *Atmospheric Chemistry and Physics: From Air Pollution to Climate Change*, 2nd ed., 1232 pp., John Wiley, Hoboken, N. J.

Sjogren, S., M. Gysel, E. Weingartner, M. R. Alfarra, J. Duplissy, J. Cozic, J. Crosier, H. Coe, and U. Baltensperger (2008), Hygroscopicity of the submicrometer aerosol at the high-alpine site Jungfraujoch, 3580 m a.s.l., Switzerland, *Atmos. Chem. Phys.*, *8*, 5715–5729, doi:10.5194/acp-8-5715-2008.

Spracklen, D. V., et al. (2010), Explaining global surface aerosol number concentrations in terms of primary emissions and particle formation, *Atmos. Chem. Phys.*, *10*, 4775–4793, doi:10.5194/acp-10-4775-2010.

Stohl, A., M. Trainer, T. B. Ryerson, J. S. Holloway, and D. D. Parrish (2002), Export of NO_y from the North American boundary layer during NARE 96 and NARE 97, *J. Geophys. Res.*, *107*(D11), 4131, doi:10.1029/2001JD000519.

Stohl, A., C. Forster, A. Frank, P. Seibert, and G. Wotawa (2005), Technical note: The Lagrangian particle dispersion model FLEXPART version 6.2, *Atmos. Chem. Phys.*, *5*, 2461–2474, doi:10.5194/acp-5-2461-2005.

Sturm, P., B. Tuzson, S. Henne, and L. Emmenegger (2013), Tracking isotopic signatures of CO_2 at the high altitude site Jungfraujoch with laser spectroscopy: Analytical improvements and representative results, *Atmos. Meas. Tech.*, *6*, 1659–1671, doi:10.5194/amt-6-1659-2013.

Tuzson, B., S. Henne, D. Brunner, M. Steinbacher, J. Mohn, B. Buchmann, and L. Emmenegger (2011), Continuous isotopic composition measurements of tropospheric CO_2 at Jungfraujoch (3580 m a.s.l.), Switzerland: Real-time observation of regional pollution events, *Atmos. Chem. Phys.*, *11*, 1685–1696, doi:10.5194/acp-11-1685-2011.

Uglietti, C., M. Leuenberger, and D. Brunner (2011), European source and sink areas of CO_2 retrieved from Lagrangian transport model interpretation of combined O_2 and CO_2 measurements at the high alpine research station Jungfraujoch, *Atmos. Chem. Phys.*, *11*, 8017–8036, doi:10.5194/acp-11-8017-2011.

Venzac, H., K. Sellegri, P. Villani, D. Picard, and P. Laj (2009), Seasonal variation of aerosol size distributions in the free troposphere and residual layer at the puy de Dôme station, France, *Atmos. Chem. Phys.*, *9*, 1465–1478, doi:10.5194/acp-9-1465-2009.

Verheggen, B., J. Cozic, E. Weingartner, K. Bower, S. Mertes, P. Connolly, M. Gallagher, M. Flynn, T. Choularton, and U. Baltensperger (2007), Aerosol partitioning between the interstitial and condensed phase in mixed-phase clouds, *J. Geophys. Res.*, *112*, D23202, doi:10.1029/2007JD008714.

Wacker, S., J. Gröbner, C. Zysset, L. Diener, P. Tzoumanikas, A. Kazantzidis, L. Vuilleumier, R. Stöckli, S. Nyeki, and N. Kämpfer (2015), Cloud observations in Switzerland using hemispherical sky cameras, *J. Geophys. Res. Atmos.*, *120*, 695–707, doi:10.1002/2014JD022643.

Weber, J. R., P. H. McMurry, F. L. Eisele, and D. J. Tanner (1995), Measurements of expected nucleation precursors species and 3–500 nm diameter particles at Mauna Loa, Hawaii, *J. Atmos. Sci.*, *52*, 2242–2257, doi:10.1175/1520-0469(1995)052<2242:MOENPS>2.0.CO;2.

Wehner, M. F., et al. (2014), The effect of horizontal resolution on simulation quality in the Community Atmospheric Model, CAM5.1, *J. Adv. Model. Earth Syst.*, *6*, 980–997, doi:10.1002/2013MS000276.

Weingartner, E., S. Nyeki, and U. Baltensperger (1999), Seasonal and diurnal variation of aerosol size distributions ($10 < D < 750$ nm) at a high-alpine site (Jungfraujoch 3580 m asl), *J. Geophys. Res.*, *104*, 26,809–26,820, doi:10.1029/1999JD900170.

Wernli, H., and H. C. Davies (1997), A Lagrangian-based analysis of extratropical cyclones. I: The method and some applications, *Q. J. R. Meteorol. Soc.*, *123*, 467–489, doi:10.1256/smsqj.53810.

Whittlestone, S., and W. Zahorowski (1998), Baseline radon detectors for shipboard use: Development and deployment in the First Aerosol Characterization Experiment (ACE 1), *J. Geophys. Res.*, *103*, 16,743–16,751, doi:10.1029/98JD00687.

Wiedensohler, A., et al. (2012), Mobility particle size spectrometers: Harmonization of technical standards and data structure to facilitate high quality long-term observations of atmospheric particle number size distributions, *Atmos. Meas. Tech.*, *5*, 657–685, doi:10.5194/amt-5-657-2012.

Wuesthoff, T. (2011), *Weather Type Classification at MeteoSwiss—Introduction of New Automatic Classification Schemes*, 46 pp., Bundesamt für Meteorologie und Klimatologie, MeteoSchweiz, Zürich, Switzerland.

Zanis, P., A. Ganser, C. Zellweger, S. Henne, M. Steinbacher, and J. Staehelin (2007), Seasonal variability of measured ozone production efficiencies in the lower free troposphere of central Europe, *Atmos. Chem. Phys.*, *7*, 223–236, doi:10.5194/acp-7-223-2007.

Zellweger, C., J. Forrer, P. Hofer, S. Nyeki, B. Schwarzenbach, E. Weingartner, M. Ammann, and U. Baltensperger (2003), Partitioning of reactive nitrogen (NO_y) and dependence on meteorological conditions in the lower free troposphere, *Atmos. Chem. Phys.*, *3*, 779–796, doi:10.5194/acp-3-779-2003.

Zellweger, C., C. Hüglin, J. Klausen, M. Steinbacher, M. Vollmer, and B. Buchmann (2009), Inter-comparison of four different carbon monoxide measurement techniques and evaluation of the long-term carbon monoxide time series of Jungfraujoch, *Atmos. Chem. Phys.*, *9*, 3491–3503, doi:10.5194/acp-9-3491-2009.